Physics – Uspekhi **59** (6) 531 – 557 (2016)

REVIEWS OF TOPICAL PROBLEMS PACS numbers: 87.15.ht, 87.15.M –, 87.15.R –

Physical stage of photosynthesis charge separation

A G Yakovlev, V A Shuvalov

DOI: 10.3367/UFNe.2016.02.037701

Contents

Abstract. An analytical review is given concerning the biophysical aspects of light-driven primary charge separation in photosynthesis reaction centers (RCs) which are special pigment-protein complexes residing in a cell membrane. The primary (physical) stage of charge separation occurs in the pico- and femtosecond ranges and consists of transferring an electron along the active A-branch of pigments. The review presents vast factual material on both the general issues of primary photosynthesis and some more specific topics, including (1) the role of the inactive B-branch of pigments, (2) the effect of the protein environment on the charge separation, and (3) the participation of monomeric bacteriochlorophyll B_A in primary electron acceptance. It is shown that the electron transfer and stabilization are strongly influenced by crystallographic water and tyrosine M210 molecules from the nearest environment of B_A. A linkage between collective nuclear motions and electron transfer upon charge separation is demonstrated. The nature of the high quantum efficiency of primary charge separation reactions is discussed.

Keywords: photosynthesis, reaction center, charge separation, electron transfer

List of abbreviations

ΔA — a change in absorption (light–darkness); BChl — bacteriochlorophyll; B_A (B_L) and B_B (B_M) — monomeric BChl in A- and B-branches, respectively; *Blc.* — *Blastochloris*; BPheo — bacteriopheophytin; *Cfx.* — *Chloroflexus*; Chl — chlorophyll; H_A (H_L) and H_B (H_M) — BPheo in A- and B-branches, respectively; Pheo — pheophytin; P — primary electron donor, BChl dimer; P^* — excited state of P; P_A (P_L) and P_B (P_M) — BChl molecules in P; Q_A and Q_B — primary and secondary quinones, respectively; RC — reaction center; *Rba.* — *Rhodobacter*; Φ_B — BPheo molecule introduced instead of B_B.

A G Yakovlev Lomonosov Moscow State University, Belozersky Research Institute of Physico-Chemical Biology,
Leninskie gory 1, str. 40, 119992 Moscow, Russian Federation
Fax +7 (495) 939 31 81
E-mail: yakov@genebee.msu.su
V A Shuvalov Lomonosov Moscow State University, Belozersky Research Institute of Physico-Chemical Biology,
Leninskie gory 1, str. 40, 119992 Moscow, Russian Federation;
Institute of Fundamental Problems of Biology,
Russian Academy of Sciences,
ul. Institutskaya 2, 142292 Pushchino, Moscow region,
Russian Federation
Fax +7 (496) 779 05 32
E-mail: shuvalov@issp.serpukhov.su

Received 19 October 2015, revised 28 January 2016
Uspekhi Fizicheskikh Nauk **186** (6) 597 – 625 (2016)
DOI: 10.3367/UFNr.2016.02.037701
Translated by Yu V Morozov; edited by A Radzig

1. Introduction

Photosynthesis constitutes a biological process in which solar energy is converted into the energy of stable chemical compounds. Photosynthesis in higher plants and algae is the main source of oxygen and organic compounds on Earth consumed as foods by animals and humans and stored underground as fossil hydrocarbon reserves. Solar energy refers to a practically inexhaustible and ecologically pure form of energy. Photosynthesis research is of primary importance from both the theoretical and applied points of view.

Photosynthesis presents a combination of the most complicated physical and chemical transformations starting from absorption of light quanta in light-harvesting chlor-

ophyll complexes. Then, the excitation energy is transferred to the so-called photosynthetic reaction centers (RCs), which are actually special pigment–protein complexes residing in a cell membrane.

The advent of laser spectrometers providing an ultrahigh temporal resolution together with the development of targeted mutagenesis techniques and X-ray analysis of the 3D structure of certain RCs greatly promoted insights into the early stages of photosynthesis. The fundamental data thus obtained make up the foundation of a modern vision of the world.

A series of fast reactions of excitation transfer to RCs results in primary conversion of the light energy into the energy of separated charges with an extremely high quantum efficiency ($\sim 100\%$) and high enough energy efficiency. The universal character of the RC structure and function in all known photosynthetic organisms is due to primary charge separation between the singlet-excited primary electron donor P and chlorophyll derivatives.

It is impossible to cover all aspects of such a unique and grandiose phenomenon as photosynthesis in the framework of a single article. We confine ourselves to a discussion of certain key issues having a long history of research and still remaining in the focus of attention. This review is focused on the primary (physical) stage of charge separation in RCs of well-known photosynthetic bacteria, which occurs in the pico- and femtosecond ranges and consists in transferring an electron along the active branch of pigments.

Section 2 is designed to report data on the RC structure and function and charge separation in them. This widely known information is presented here to prepare the reader for considering more special problems in Sections 3–5. The sophisticated reader can refer directly to any of these three sections and look through them in any order, because each is actually a self-contained portion of the review. Some general issues are first discussed in Section 2 and thereafter (in more detail) in Sections 3–5.

X-ray diffraction analysis of crystals in certain RCs yielded comprehensive information on their spatial structure. Traditional physico-chemical methods for RC investigations are now supplemented by such new techniques as femtosecond spectroscopy of genetically modified objects. Figure 1 illustrates the RC structure of the purple bacterium *Rhodobacter* (*Rba.*) *sphaeroides*, a classical study object. Charge separation in these RCs occurs along the photoactive A-branch of pigments and consists in transferring an electron from the excited bacteriochlorophyll dimer P^* to bacteriopheophytin H_A for approximately 3 ps and thereafter from H_A^- to quinone Q_A for ~ 200 ps. The quantum effectiveness of charge separation in RCs is close to 100%.

Section 3 deals with selected aspects of research on the role of the inactive B-branch of pigments. It follows from Fig. 1 that each RC pigment has two symmetric branches, but charge separation occurs virtually along the single active branch. This enigmatic inconsistency has drawn the steadfast attention of researchers for many years, the main approach to addressing this issue being activation of electron transfer along the B-branch by site-directed mutagenesis. A few prerequisites for B-branch inactivity have been revealed, viz. the position of the $P^+B_B^-$ energy level well above the P^* level, a stronger electronic conjugation between P^* and B_A than that between P^* and B_B, and a much higher positive potential of the A-branch compared to that of the B-branch. Moreover, a reversible coherent transfer of an electron to the B-branch is

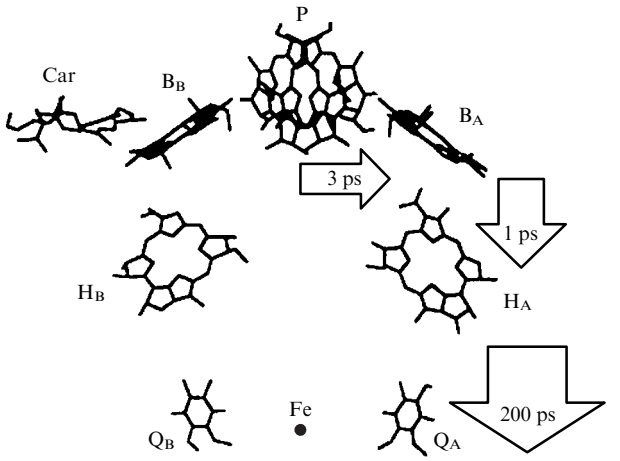

Figure 1. Spatial structure of *Rba. sphaeroides* RCs according to the PDB databank, file 1AIJ. The figure shows $BChlP_A$ and P_B molecules forming a P dimer, monomeric BChl B_A and B_B molecules, BPheo H_A and H_B molecules, quinone Q_A and Q_B molecules, an iron atom, and carotinoid molecule (Car). Arrows schematically indicate the electron transfer pathway.

possible under the effect of the movement of a vibrational wave packet. This transfer starts a few dozen femtoseconds earlier than the analogous coherent transfer of an electron along the photoactive A-branch. The coherent electron transfer in the B-branch is unrelated to the presence or absence of conditions for a usual incoherent transfer and is largely determined by wave packet dynamics.

Section 4 is devoted to selected aspects of such a multifaceted problem as the influence of the RC pigment environment on charge separation. The pigments depicted in Fig. 1 are inbuilt in a protein matrix composed of amino acid residues combined into protein subunits. The pigment environment contains a few hundred water molecules, besides protein. The spatial structure of RCs is maintained by virtue of numerous van der Waals interactions between pigments and protein and by several hydrogen bonds. In addition, the nearest environment of pigment molecules influences primary charge separation by altering the energy characteristics of electron transfer reactions or as a constituent part of the electron transfer pathway.

Two of the numerous molecules of the pigment environment are especially interesting: tyrosine (Tyr) M210, and bound water HOH55 (notations of the molecules are given for RCs of *Rba. sphaeroides*) located near B_A. The absence of these molecules significantly slows down charge separation in RCs. Numerous data suggest the key role of tyrosine M210 in stabilization of separated charges in the $P^+B_A^-$ state, which is maintained by the polar OH group of Tyr M210 and its reorientation under the effect of separated charges. Water HOH55 can be involved in one of the spatial effective electron transfer pathways along the chain of polar atomic groups connecting the P dimer and B_A monomer. In the absence of HOH55, electron transfer occurs along different, less efficient spatial pathways.

Section 5 concerns with the participation of monomeric bacteriochlorophyll B_A in primary charge separation. This problem has a long history and logically ensues from the position of B_A between P and H_A, as revealed by X-ray structural analysis (see Fig. 1). The first indirect data on the possibility of electron transfer to B_A were obtained 30 years

ago. Then, no conclusive evidence of direct B_A involvement in charge separation could be obtained for many years. Little by little, results of pico- and femtosecond spectroscopy contributed to better understanding the main difficulty behind observation of the $P^+B_A^-$ state, which proved to be its low population. Another difficulty was that the $P^+B_A^-$ state spectrum was strongly masked by the spectra of other states in the visible region, where the overwhelming majority of measurements were made. The existence of the $P^+B_A^-$ state was convincingly proved by measurements in the near-IR range, where B_A^- anions showed a weak 1020-nm absorption band. At the beginning, this band was studied in chemically modified RCs, where a blockade of electron transfer to H_A resulted in the accumulation of the $P^+B_A^-$ state population in the picosecond range. Today, the two-step electron transfer scheme $P^* \rightarrow P^+B_A^- \rightarrow P^+H_A^-$, with the latter reaction being several-fold faster than the former, is universally accepted.

2. General information on photosynthetic processes

2.1 Elementary representation of photosynthesis

The generalized reaction of photosynthesis in plants, cyanobacteria, and eukaryotic algae can be schematically represented as

$$6CO_2 + 6H_2O + \text{light} \rightarrow 6O_2 + (CH_2O)_6\,,$$

with O_2 being liberated from water molecules. The simplicity of this reaction is delusive. Real photosynthesis constitutes a very complicated process physically based on energy and charge transport. Photosynthesis starts from light absorption in light-harvesting complexes composed of chlorophyll molecules (bacteriochlorophyll). Their number varies in different objects from a few dozen to several thousand.

The excitation energy migrates inside a complex till it reaches the photosynthetic RCs (see Section 2.2). Characteristic migration time ranges from tens to hundreds of picoseconds. The primary charge separation (into an electron and a hole) in an RC takes a few picoseconds. An electron leaving an RC enters the electron transport chain, where its energy is spent to synthesize chemical compounds. Thus, photosynthesis provides the conversion of light energy into the energy of chemical bonds of end products (glucose).

The processes of water decomposition and CO_2 assimilation occur separately in the chloroplasts of plant cells. An important role in water decomposition is played by electron transfer in RCs and along the chain of its carriers inside a chloroplast membrane. Electron detachment from a water molecule results in reduction of oxidized nicotinamide adenine dinucleotide phosphate ($NADP^+$) and synthesis of adenosine triphosphate (ATP). Further on, reduced NADP (NADPH) and ATP participate in maintaining CO_2 assimilation and carbohydrate synthesis.

The source of electrons in photosynthetic bacteria is a donor stronger than water, e.g., H_2S. Unlike bacteria, plants and algae have two types of photosystems, short- and long-wavelength (photosystems II and I, respectively). Accordingly, there are two types of RCs containing P680 and P700 pigments. In conformity with the so-called Z-scheme, an electron ascends against the thermodynamic gradient, while two light quanta are successively absorbed by the two photosystems. Photosystem II is responsible for water decomposition. The excited P680 pigment gives up an electron to plastoquinone and further on to the chain of its membrane transporters. One of these carriers, plastocyanine, donates the electron to the $P700^+$ pigment that, being light excited, transfers it to ferredoxin and then to $NADP^+$. In bacterial photosynthesis, an electron is transferred from the excited bacteriochlorophyll dimer to ubiquinone. Then, the electron can either return to the oxidized dimer (cyclic transport in the absence of an external electron donor) or reduce the ubiquinone pool (in the presence of an external donor).

Reduction of $NADP^+$ in bacteria occurs in the course of back transfer of an electron and is accompanied by hydrolysis of ATP molecules. ATP is synthesized as a proton concentration gradient forms on both sides of the cellular membrane with embedded RCs. These protons are transferred across the membrane and released inside it. Approximately two protons per electron are absorbed on the inner side of the membrane as $NADP^+$ is reduced on its outer side.

Notice that light-harvesting complexes, RCs, and components of the electron transport chain in higher plants are embedded into a thylakoid membrane composed primarily of lipids and enclosed in chloroplast grana. In bacteria, the photosynthetic apparatus is formed by protrusions of the inner cellular membrane.

2.2 Structure of bacterial reaction centers

The reaction center of bacterial photosynthesis involves a pigment-protein complex responsible for the conversion of light energy into the energy of separated charges in a series of rapid electron transfer events. The structure, function, and mechanism of charge separation have been thoroughly explored in RCs of purple photosynthetic bacteria. Relevant data and a detailed bibliography can be found in numerous reviews, articles, and monographs (e.g., Refs [1–13]).

RCs of purple photosynthetic bacteria contain the following chromophores involved in light absorption and electron transfer: four bacteriochlorophyll (BChl) molecules, two bacteriopheophytin (BPhe) molecules, and two quinone (Q) molecules (ubiquinone or menaquinone). The structural basis of BChl and BPheo molecules is a flat tetrapyrrole ring. In the BChl molecule, four nitrogen atoms of pyrrole rings ligate to the central Mg^{2+} atom. In the BPheo molecule, the Mg^{2+} atom is replaced by two hydrogen atoms. The periphery of the tetrapyrrole ring in the BChl molecule is occupied by various substituents, including a cyclopentane ring and a hydrophobic branch (phytol). RCs of purple bacteria containing a-type (BChla) and b-type (BChlb) BChl molecules [14] are formed by three protein subunits (light L, medium M, and heavy H) with a molecular mass from 24 to 32 kDa that include four BChl molecules, two BPheo molecules, two Q molecules, and one iron atom. The BChl, BPheo, and Q molecules are enclosed in L- and M-subunits of protein [15–17]. The RCs of certain bacteria include cytochrome containing one protein subunit and four hemes [16, 17]. RCs of green bacteria *Chloroflexus* (*Cfx.*) *aurantiacus* have two protein subunits with a mass of $\approx$ 26 kDa [18], three BChl molecules, three BPheo molecules [19], and two menaquinones [20].

The data on the primary sequence of L- and M-subunits [21] together with the results of X-ray diffraction analysis of RC crystals [16, 17, 22–27] allowed elucidating the RC overall

spatial structure (see Fig. 1). L- and M-subunits of RCs from *Blastochloris* (*Blc.*) *viridis* contain 273 and 323 amino acid residues, respectively. The hydrophobicity profile of L- and M-subunits exhibits five segments intersecting the membrane. They make up α-helices (a, b, c, d, e) lying roughly parallel to one another and forming a structure with C_2-symmetry. The LM complex is closed by cytochrome on the side of periplasm, and by the H-subunit on the side of cytoplasm. BChl and BPheo molecules are located in the vicinity of c, d, and e α-helices in L- and M-subunits. Dimeric BChl (P) is the primary electron donor formed by two molecules, P_L and P_M, in which the central magnesium atom is ligated by histidine (His) molecules L173 and M200. These molecules are localized on α-helices nearer to the region closed by the cytochrome protein. The BChl (P) macrocycle planes lie above each other and overlap orbitals of the first pyrrole rings, with the minimal distance between the planes being only ~ 3 Å. Such apposition creates conditions for the strong exciton interaction with an energy of around 600 cm^{-1} [28–30] responsible for manifesting specific spectral and redox properties of P.

Two molecules of monomeric BChl, B_L and B_M, are ligated to His L153 and His M180, respectively, in the vicinity of the chains connecting c and d α-helices. The minimal distance between $B_{L,M}$ and P macrocycles is 3.5 Å, while the distance between the centers of P and $B_{L,M}$ is around 13 Å. There are BPheo molecules, H_L and H_M, in the center of the protein hydrophobic region between c and e α-helices. The distance between the centers of P and $H_{L,M}$ reaches ≈ 17 Å, and that between $B_L(B_M)$ and $H_L(H_M)$ is ≈ 11 Å. The end acceptors Q_A (in the M-subunit) and Q_B (in the L-subunit) are located between the c and e α-helices nearer to the region closed by the H-subunit of the RC protein. Q_A is found in contact with the triptophane (Trp) molecule M252, and Q_B with the phenylalanine (Phe) L216 molecule. These two molecules are located in the vicinity of the chains connecting d and e α-helices and simultaneously penetrate toward α-helices of the symmetrical subunits. There is an iron atom between Q_A and Q_B, which is ligated by His L190, L230, M217, and M264 molecules of d and c α-helices in L- and M-subunits. These His molecules are located nearer to the region closed by the H-subunit. The chromophores nearest to Q_A and Q_B are H_L and H_M, respectively.

It follows from the above that an RC contains two symmetrically related chains of cofactors, $P_L/B_L/H_L/Q_A$ and $P_M/B_M/H_M/Q_B$, which join together both in the region of overlapping between P_L and P_M orbitals and near the bridge formed by the iron atom between Q_A and Q_B (see Fig. 1). The rigid backbone for cofactor chains is formed by α-helices of protein. In such a structure, the distance and interaction between prosthetic groups are practically independent of temperature.

The total charge in M- and L-subunits is −8 on the side of the periplasm, and +6 on the side of the cytoplasm. Once the charge of the Fe^{2+} atom is taken into consideration, the total charge on the side of the cytoplasm equals +8. The position of these charges is such that it favors electron transfer from P to Q_A.

The general distribution of amino acid residues around P promotes displacement of electrons toward P_L due to the asymmetric arrangement of polar and nonpolar residues.

B_L and B_M molecules are in van der Waals contact simultaneously with P, H_L, and H_M molecules. His L153 and His M180 molecules ligate Mg^{2+} atoms in B_L and B_M, respectively. Moreover, B_L and B_M molecules are in multiple van der Waals contacts without forming H-bonds.

BChl molecules in P lie in the planes forming an angle of about 10° to each other. The angle between the lines connecting N_1 and N_3 atoms in each of the two BChl molecules in P approaches $\approx 140°$, which ensures an optimal overlap between the first pyrrole cycles of these BChl. The distance between the pyrrole cycles of two BChl molecules in P is around 3.5 Å.

The B_L molecule in RCs of *Rba. sphaeroides* and *Blc. viridis* occupies the place between P and H_L, while the B_M molecule is between P and H_M. The van der Waals overlap for B_L and P_M orbitals is 1.5 times that for B_M and P_L; it is one of the factors responsible for the predominant electron transfer along the A-branch.

2.3 Primary charge separation in reaction centers

The primary donor of electrons in RCs of photosynthetic purple bacteria is the bacteriochlorophyll (BChl) dimer P. Its main absorption band lies within the 865–885-nm range in *BChla-containing Rhodobacter* (*Rba.*) *sphaeroides, Rba. capsulatus, Chromatium vinosum, and Thermochromatium tepidum*, and at ≈ 960 nm in *BChlb-containing Blastochloris* (*Blc.*) *viridis*. Excitation of P causes it to move into the first excited singlet state P^* from which an electron is transferred to a bacteriopheophytin (BPheo) molecule, thus giving rise to forming the $P^+H_A^-$ state. Then, the electron passes from H_A^- to quinone (Q_A), from which it further moves to secondary quinone Q_B. Oxidized P^+ receives the electron from the c-type cytochrome and the process of transmembrane electron transfer repeats itself. At room temperature, electron transfer from P^* to H_A takes 3–5 ps in RCs of *Rba. sphaeroides* and *Rba. capsulatus*, and about 2 ps in RCs of *Blc. viridis* [31–44]. Electron transfer from H_A^- to Q_A takes approximately 200 ps [45–47]. The time constant of electron transfer from cytochrome to P^+ varies from 0.5 to 50 μs, depending on the type of RC.

According to the general theory of charge separation [1–13], the rate constant k_{DA} of electron transfer from donor D to acceptor A depends on the transmission coefficient $\sigma(r)$ determining the probability of an electron moving from D^* to A in one pass toward the intersection region between D^*A and D^+A^- potential surfaces at a fixed distance r. This coefficient varies roughly as $\exp[-\beta(r-r_0)]$, where β lies in the range from 1 to 2 $Å^{-1}$, where r_0 is the distance at which $\sigma(r)\upsilon = 10^{13}\ s^{-1}$, and υ is the frequency factor. Also, the expression for k_{DA} contains the exponential factor $\exp[-E_a/(k_BT)]$, where E_a is the free activation energy, k_B is the Boltzmann constant, and T is temperature:

$$k_{DA} = \sigma(r)\,\upsilon \exp\left(-\frac{E_a}{k_BT}\right). \qquad (1)$$

The reverse reaction rate constant k_{AD} is expressed as $k_{AD} = k_{DA}\exp[\Delta G/(k_BT)]$, where ΔG is the free energy of the reaction. If the energy of the state D^+A^- is lower than the energy of D^*A, then $\Delta G < 0$ and $k_{AD} < k_{DA}$.

In the case of a strong electronic conjugation between the two states (adiabatic reaction), the value of $\sigma(r)$ is close to unity, and υ takes the meaning of the effective frequency for nuclear motion along the reaction coordinate.

If $\sigma(r) \ll 1$ (nonadiabatic case), the expression for the electron transfer rate constant can be derived by quantum-mechanical calculations. In this case, the rate constant of

electron transfer (k) in the first approximation in the high-temperature limit is expressed as

$$k = 2\pi\hbar^{-1}V^2(4\pi E_r k_B T)^{-0,5}\exp\left(-\frac{E_a}{k_B T}\right), \quad (2)$$

where $\hbar$ is the Planck constant, V is the matrix element of electronic conjugation, and E_r is the reaction reorganization energy. The activation energy E_a is related to the reorganization energy E_r and the free energy ΔG of the reaction by the expression

$$E_a = 0.25E_r\left(1+\frac{\Delta G}{E_r}\right)^2. \quad (3)$$

It follows from formula (3) that the activation barrier disappears at $\Delta G = -E_r$, i.e., when the D^+A^- potential curve intersects the analogous D^*A curve at its minimum. In this case, the reaction rate constant reaches a maximum.

Formula (2), although approximate, is widely used to estimate charge separation and transfer rate constants. For the primary $P^* \rightarrow P^+B_A^-$ reaction in RCs of *Rba. sphaeroides* at $\Delta G \approx -500$ cm^{-1} and $E_r \approx 650$ cm^{-1}, the barrier is very small: $E_a \approx 9$ cm^{-1}. If we set $V \approx 20$ cm^{-1}, then $k \approx 1/(3$ ps) at $T = 293$ K and $k \approx 1//(1.7$ ps) at $T = 90$ K, i.e., close to experimental values. For the $P^+B_A^- \rightarrow P^+H_A^-$ reaction in RCs of *Rba. sphaeroides*, the barrier is equally very low: at $\Delta G \approx -1500$ cm^{-1} and $E_r \approx 1500$ cm^{-1}, one has $E_a \sim 0$. For this reaction, the theoretical rate constant $k \approx 1/(0.3$ ps) at $T = 90$ K, similar to the observed one, is obtained at $V \approx 40$ cm^{-1}.

In native RCs, only the A-branch of cofactors participates in electron transfer [48–57]. In wild-type RCs, electron transfer from P^* to H_B is not detected, as shown by spectroscopy of the H_B absorption band differing from the analogous H_A band. The spectral difference between these bands arises from the fact that the hydrogen bond with a protonated Glu residue (glutamic acid) displaces H_A absorption bands Q_x and Q_y toward the long-wavelength region relative to the analogous H_B bands [58]. Hereinafter, Q_x and Q_y are the spectroscopic notations for long-wavelength molecular transitions polarized along the mutually perpendicular x- and y-axes. These axes are usually chosen such that they lie in the plane of the tetrapyrrole ring of chlorophyll or bacteriochlorophyll molecules.

The high rate constant of primary electron transfer reactions may be due to the small distance (on the order of 3–4 Å) between certain B_A atoms of the π-system and P and H_A atoms. The quantum yield of charge separation is close to unity [59–61]. The electron transfer rate increases as temperature drops [33, 34, 41, 44, 62–67]. At 20 K, the time constant of $P^+H_A^-$ formation is around 1.2 ps in RCs of *Rba. sphaeroides*, and some 0.9 ps in RCs of *Blc. viridis*. Electron transfer from H_A^- to Q_A is also accelerated approximately two-fold as temperature decreases [68–70].

The main peaks in the absorption spectra of unexcited RCs of *Rba. sphaeroides*, corresponding to Q_y and Q_x transitions, are produced by P (wavelength $\lambda = 865$ nm at 293 K), $B_{A,B}$ (800 nm), and $H_{A,B}$ (760 nm). The 595-nm band results from the contribution from both P and $B_{A,B}$, whereas the 540-nm band is formed by $H_{A,B}$. At low temperatures, the P band shifts to 890 nm and becomes roughly 1.5 times narrower. An H_B band and an H_A band can be distinguished in the 540-nm band at 533 nm and 546 nm, respectively. In the wide Soret band, the contribution from H in its short-wavelength part and from P in the long-wavelength part can be singled out [71]. The carotinoid molecule performing light-harvesting and photoprotective functions shows a low peak at 500 nm [72]. Fluorescence and stimulated emission from P^* have a maximum near 915–920 nm. The replacement of BPheo by the a-type plant pheophytin leads to the disappearance of 760-nm bands and the appearance of a 670-nm band of plant pheophytin. Formation of P^+ cation-radical results in the disappearance of the initial 865- and 590-nm P absorption bands and the appearance of a wide band in the IR region of the spectrum with a maximum at 1250 nm. The appearance of the H_A^- anion-radical is associated with the disappearance of 762- and 546-nm absorption bands substituted by wide 650-, 920-, and 960-nm absorption bands. The formation of H_A^- for RCs with BChlb is apparent from altered absorption in the wavelength range from 790 to 830 nm. Formation of a B_A^- anion-radical leads to the disappearance of B_A absorption bands at 800 and 595 nm and the appearance of a weak 1020-nm band. Characteristic absorption bands become shifted upon chemical or genetic modification of RCs, but no consistent patterns of such displacement have been elucidated yet [73]. An impact on the H-bond with the H_A ketogroup causes a shift in the 760-nm band [58]. The P absorption band can shift toward the short wavelength region by approximately 15 nm as a result of mutations affecting the H-bond with the acetyl group. Considerable changes in the RC absorption spectrum are observed after replacement of cofactors caused by mutations [74, 75].

Similar to the RCs of purple bacteria, RCs of thermophilic green bacteria *Cfx. aurantiacus* consist of dimeric BChl as the primary electron donor, BPheo as the intermediate acceptor of electrons, and two menaquinone molecules, Q_A and Q_B [18, 20,76–81]. The 3D structure of these RCs remains to be elucidated. A comparison of the polypeptide structure, spectroscopic data, and results of calculations in the framework of the exciton theory indicates that cofactors in RCs of *Cfx. aurantiacus* form two pigment chains, as they do in RCs of *Rba. sphaeroides* [80, 82–88].

It was shown that the rate constant of electron transfer to H_A in RCs of *Cfx. aurantiacus* is lower than in RCs of *Rba. sphaeroides* [89, 90]. At 296 K, P^* degradation occurs with a time constant of 7 ps; at 10 K, two components are distinguishable in degradation kinetics with time constants 2 and 24 ps, respectively. Quantum yields of primary charge separation at 280 K [91] and room temperature [92] are close to unity. It can be speculated that an additional BChl molecule, B_A, participates in electron transfer from P^* to H_A as a mediator [86, 92]. Further electron transfer from H_A^- to primary quinone Q_A with the generation of the $P^+Q_A^-$ state occurs in RCs of *Cfx. aurantiacus* with a time constant of ~ 320 ps at 280 K [79].

Although RCs of *Cfx. aurantiacus* are similar to other bacterial RCs as far as chromophore arrangement and photochemical properties are concerned, they are essentially different in terms of protein and cofactor compositions [76]. Certain amino acid residues present in the RCs of purple bacteria are absent in RCs of *Cfx. aurantiacus*. For example, the RCs of *Cfx. aurantiacus* contain leucine (Leu) instead of Tyr M210, which probably explains the slow-down of primary charge separation.

To recall, the B-branch in RCs of *Cfx. aurantiacus* includes two BPheo molecules, Φ_B and H_B, with Φ_B occupying the position of B_B [19, 79]. The level of the $P^+B_B^-$

state free energy in purple bacteria lies 0.24 eV higher the P^* energy level, whereas that of the $P^+B_A^-$ state is somewhat lower than the P^* energy level [93, 94]. This difference in free energy levels is believed to be an important factor accounting for the functional inactivity of the B-branch.

The *in vitro* midpoint potential of a BPheo/$BPheo^-$ redox couple is 0.23–0.30 eV higher than that of a BChl/$BChl^-$ couple [95, 96]. This facilitates reduction of BPheo-a Φ_B in comparison with BChla B_B. On the other hand, the midpoint redox potential of a P/P^+ redox couple in RCs from *Cfx. aurantiacus* is 70–90 mV lower than in RCs from *Rba. sphaeroides* [77, 86], meaning that the $P^+\Phi_B^-$ energy level in RCs of *Cfx. aurantiacus* can be close to and even lower than that of P^*, which makes possible electron transfer along the B-branch.

The authors of Ref. [97] tried to explain the low-temperature kinetics of fluorescence in RCs of *Cfx. aurantiacus* with reduced Q_A and arrived at the conclusion that the rapid reversible electron transfer between P^* and BPheo along the B-branch appears possible. However, results of differential absorption spectroscopy in the Q_x band of BPheo molecules and the close-to-unity quantum yield of primary charge separation in RCs of *Cfx. aurantiacus* give evidence of the prevalent electron transfer along the A-branch [91, 92, 98].

A different sequence of primary reactions is observed after direct excitation of B_A or H_A [99–101]. A similar effect occurs in the case of multiphoton [102] and blue light [103] excitation of RCs. The B_A^* energy level being higher than that of P^*, a direct $B_A^* \rightarrow P^+B_A^-$ reaction becomes possible and is especially quite apparent in RCs of the YM210F mutant at low temperatures when the $P^* \rightarrow P^+B_A^-$ reaction is considerably slowed down. Moreover, B_A^* transfers the excitation energy to P with a time constant of ~ 100 fs. A direct $B_A^* \rightarrow P^+H_A^-$ reaction may proceed under certain conditions. At the same time, some authors question the important role of the B_A^* state in fast electron transfer [104–106].

The primary charge separation in RCs is accompanied by a loss of electron energy. For example, the energy of the $P^+H_A^-$ state is roughly 0.2 eV lower than the P^* energy; the difference increases to approximately 0.65 eV for the $P^+Q_A^-$ state, which is equivalent to almost 50% of the initial energy of an absorbed light quantum. The energy efficiency of primary charge separation in different types of RCs amounts to 50–60%. This value is much higher than the efficiency factor of modern artificial semiconductor solar energy converters, even if it is not the highest possible. The energy of the $P^+B_A^-$ state formed before $P^+H_A^-$ is roughly 0.07 eV lower than the P^* energy (see Section 5 for details). Excess energy is absorbed by the pigment environment of RCs.

Subpicosecond spectroscopy data for pheophytin-modified RCs of *Rba. sphaeroides* indicate that the $P^+B_A^-$ recombination time equals ≈ 1 ns or three times as large as the lifetime of P^*B [107]. $P^+H_A^-$ recombination time is 15 ns at $T = 293$ K and 20 ns at $T = 77$ K. This means that $P^+H_A^-$ recombination proceeds almost 20 times slower than $P^+B_A^-$ recombination [108]. $P^+Q_A^-$ recombination time reaches 30 ms at $T = 77$ K, and 100 ms at $T = 293$ K, while the $P^+Q_B^-$ recombination time can be as large as several seconds [2, 7].

Thus, each new stage of electron transfer in RCs is accompanied by a loss of energy of the initially absorbed quantum in exchange for an increase in dissipation time of the energy stored during its gradual rise at each stage of charge separation. In accordance with the X-ray structural model of RCs [16, 17, 22], each electron transfer stage is accompanied by an increase in the distance between P^+ and the next acceptor: 11 Å (between the centers) for $P^+B_A^-$, 16 Å for $P^+H_A^-$, and 25 Å for $P^+Q_A^-$. In this case, the removal of an electron leads to the lowering of the interaction energy between unpaired electrons, while the velocity of their backward travel over vacant orbitals sharply decreases under the effect of the Boltzmann factor hampering electron transition to a higher energy state.

Stimulated P^* emission kinetics shows not only the main component with a time constant of 3–4 ps at 293 K, but also a minor slower component (time constant $\sim 10-20$ ps at $T = 293$ K) [43, 109–116]. The origin of the slower component is attributable to static or dynamic heterogeneity of the reaction [66, 89, 117–120], relaxation of the $P^+H_A^-$ dipole environment [34, 42, 115, 121, 122], P^* relaxation [65, 116], or reversible electron transfer into the B-branch [112]. It remains unclear whether these two components in P* kinetics correspond to two different processes or to a single non-exponential process.

Results of dip burning experiments do not confirm the hypothesis of marked RC heterogeneity [123–125]. The observed dip width and shape in RC spectra excited near the 0–0 transition at low temperatures are consistent with the P^* quenching time of around 1 ps (close to kinetic measurements). Nor do narrower-band dips in RC spectra are also observed that might correspond to the slower P^* decay. Calculations show that neither the width of the dip being burnt nor the respective electron transfer rate change significantly upon variation of the exciting light wavelength in the region of heterogeneous distribution of 0–0 transitions [123, 124]. The lack of correlation between the kinetics of electron transfer and 0–0 transition energy implies the absence of RC heterogeneity. Femtosecond IR spectroscopy revealed internal P^* relaxation with a time constant of 0.2 ps at 285 K into a different state supposedly corresponding to charge separation inside P^* [126]. Dip burning experiments at low temperatures do not confirm the P^* transition to a different state with a characteristic time substantially smaller than 1 ps [124, 127–129].

In RC excitation by light pulses of 30 fs duration or shorter, the oscillations are observed in stimulated or spontaneous emission of P^* [109, 110, 113, 130–139]. The main mechanism behind their generation is believed to be the motion of the nuclear wave packet over the surface of the P^* state potential energy. The wave packet forms as a result of simultaneous excitation of several vibrational sublevels in the P^* state. As a consequence of the displacements of the P^* and P potential energy surfaces, the motion of the wave packet is visualized as a change in the shape of the P^* stimulated emission spectrum [109, 110,130–137]. The spectrum of this motion includes a series of frequencies in the range of 10–400 cm^{-1}. The upper limit of the observed vibrational frequencies appears to be given by the spectral width of the exciting pulse. Calculations show that oscillations are equally possible in states with separated charges [140, 141].

Vibrations in $P^+B_A^-$ can be due not only to electron density transfers back onto P*, but also to rapid transitions in $P^+H_A^-$ accompanied by slower accumulation of $P^+B_A^-$ [140, 141]. The contribution of certain types of BChl motion and protein environment to P^* and $P^+B_A^-$ vibrations remains to be estimated. Experiments on resonant Raman scattering and calculations of normal vibrational modes for isotope-labelled BChl give evidence that out-of-plane strain of C2 acetyl groups has a strong mode at 35 cm^{-1}, while a series of strains

of macrocyclic rings have a 139-cm^{-1} mode [142]. Protein molecules also exhibit low-frequency modes of motion [139].

The characteristic lifetime of the wave packet ranges 1–2 ps, with high-frequency modes of its motion damping faster than low-frequency ones [133]. At low temperatures, this time is roughly equal to the lifetime of P^* in a native RC. In mutant RCs with retarded charge separation, the wave packet lifetime remains unaltered, i.e., some 1–2 ps. The wave packet lifetime may reflect the P^* vibrational relaxation, which can include both dephasing of vibrational sublevels due to energy fluctuations and transferring the excess of vibrational energy at these sublevels to the environment. If vibrational relaxation of $P^+B_A^-$ and $P^+H_A^-$ occurs with the same characteristic time as P^* relaxation (1–2 ps), it can limit the total charge separation rate [34, 42, 121, 122, 143–145]. Calculations by the probability density matrix method indicate, however, that vibrational relaxation of various RC states is fast enough not to restrict the charge separation rate, while its further acceleration may have the inverse effect, i.e., a slow-down of charge separation [140, 141].

Femtosecond spectroscopy of RCs in the 280-nm wavelength range has demonstrated changes in absorption immediately after excitation that attenuated with characteristic times of 3, 10, and 190 ps, regardless of various mutations [116]. It was conjectured that components with characteristic times of 3 and 10 ps reflect protein dielectric relaxation around P^*, and the component with a characteristic time of 190 ps is related to the $H_A^- \rightarrow Q_A$ electron transfer. Alterations of absorption at 280 nm may reflect the influence of changes in local electric fields on triptophane (Trp) amino acid residues near P, B_A, and H_A.

2.4 Efficiency of the primary photosynthetic act

Numerous experiments designed to measure quantum efficiency Φ_p (or quantum yield according to another terminology) of primary photochemical processes in RCs with the use of different methods have given a remarkable result: $\Phi_p \sim 1$ (see reviews and discussions in Refs [1–13]). This means that absorption of a single light quantum roughly corresponds to the transfer of a single electron. Even the earliest measurements of the absorption band bleaching rate in the P dimer dating back to the 1970s gave the minimal value of $\Phi_p \approx 0.98$. This result no longer seems surprising in light of the data obtained since that time, yet it continues to be admired as an example of the perfection of living nature.

Let us consider this issue in greater detail as exemplified by RCs of photosynthetic purple bacteria *Rba. sphaeroides* — a classical object of research due to its ready availability and simplicity of performing methodical procedures. The quantum efficiency of the charge separation reaction is by definition the ratio of the number of transferred electrons to the number of light quanta absorbed by donor molecules. Under stationary illumination, the number of particles absorbed per unit time becomes the issue.

In accordance with the photochemical equivalence law, each absorbed light quantum excites a single molecule (in the absence of multiphoton processes). The quantum yield of a one-step reaction can be represented as

$$\Phi_p = \frac{K_r}{K_r + \sum k}, \tag{4}$$

where K_r is the reaction rate, and $\sum k$ is the sum of rates of all other processes competing with charge separation. If charge separation is much faster than all other processes, one has $K_p \gg \sum k$ and $\Phi_p \leqslant 1$.

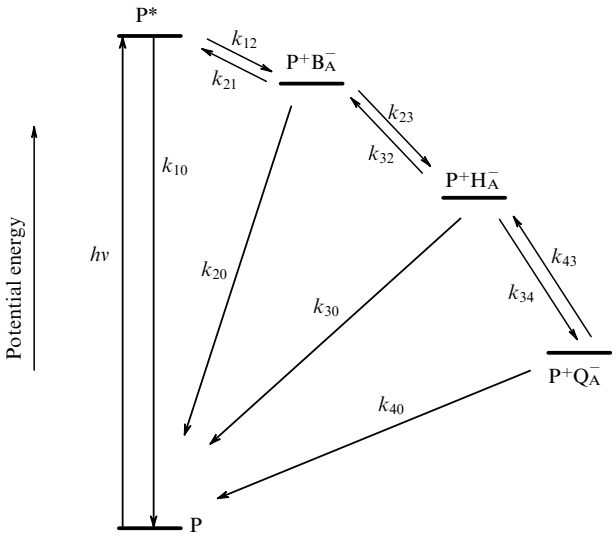

Figure 2. Diagram of energy levels and transitions between them for bacterial RC states (see the text for explanation).

The available data indicate that charge separation in bacterial RCs is a three-stage process in which four states are involved (Fig. 2). Each stage is characterized by the forward electron transfer rate $k_{i,i+1}$, the reverse rate $k_{i,i-1}$, and the rate of losses $k_{i,0}$, $i = 1-4$. In RCs of *Rba. sphaeroides*, these rates have been experimentally determined with a high accuracy (see Table 1).

Suppose that a steady-state quantum flux of light I is absorbed in RCs. The stationary populations of P^* states (N_1), $P^+B_A^-$ (N_2), $P^+H_A^-$ (N_3), and $P^+Q_A^-$ (N_4) can be found by solving the following system of kinetic equations:

$$\begin{aligned}
\frac{dN_1}{dt} &= I + k_{21}N_2 - (k_{10} + k_{12})N_1 = 0, \\
\frac{dN_2}{dt} &= k_{12}N_1 + k_{32}N_3 - (k_{21} + k_{23} + k_{20})N_2 = 0, \\
\frac{dN_3}{dt} &= k_{23}N_2 - (k_{32} + k_{34} + k_{30})N_3 = 0, \\
\frac{dN_4}{dt} &= k_{34}N_3 - (k_{43} + k_{40} + k_{bio})N_4 = 0.
\end{aligned} \tag{5}$$

In the last equation, k_{bio} is the arbitrary rate of the biochemical stage of photosynthesis; this stage is absent in isolated RCs under laboratory conditions. In this case, it is necessary to prevent accumulation of the $P^+Q_A^-$ states responsible for RC oxidation and the loss of its function by

Table 1. Transition rates (s^{-1}) in RCs of *Rba. sphaeroides*.

k_{10}	k_{20}	k_{30}	k_{40}	k_{12}	k_{21}	k_{23}	k_{32}	k_{34}	k_{43}
1.2×10^9	10^9	7×10^7	10^1	3.3×10^{11}	2.7×10^{10}	10^{12}	5.4×10^8	5×10^9	1.2×10^2

adding chemical agents known to maintain RCs in the so-called open state for which it is possible to assume that $N_4 = 0$ and disregard the last equation. The k_{10} loss is the sum of radiative and nonradiative losses. The following expression holds for the quantum yield of $P^+Q_A^-$:

$$\Phi_{1-3} = \frac{k_{34}N_3}{I} = \frac{k_{34}XY}{Z}\,, \tag{6}$$

where $X = k_{23}/(k_{32}+k_{34}+k_{30})$, $Y = k_{12}/(k_{21}+k_{23}+k_{20}-Xk_{32})$, and $Z = k_{10} + k_{12} - k_{21}Y$. Reverse reactions are linked to direct ones through the relationships $k_{21} = k_{12}\exp[-\Delta E_{12}/(k_B T)]$, $k_{32} = k_{23}\exp[-\Delta E_{23}/(k_B T)]$, and $k_{43} = k_{34}[-\Delta E_{34}/(k_B T)]$, where ΔE are the differences between the potential energies of the respective states.

The same line of reasoning leads to the following expression for the quantum yield of $P^+H_A^-$:

$$\Phi_{1-2} = \frac{k_{23}N_2}{I} = \frac{k_{23}\hat{Y}}{k_{10}+k_{12}-k_{21}\hat{Y}}\,, \tag{7}$$

where $\hat{Y} = k_{12}/(k_{21}+k_{23}+k_{20})$.

The quantum yield of $P^+B_A^-$ is given by the simple expression

$$\Phi_1 = \frac{k_{12}N_1}{I} = \frac{k_{12}}{k_{12}+k_{10}}\,. \tag{8}$$

Substituting the table values into this equation gives $\Phi_{1-3} = 0.98$, $\Phi_{1-2} = 0.995$, $\Phi_1 = 0.996$. All three stages of charge separation have a quantum yield close to unity. The largest quantum losses (about 2%) are inherent in the slowest third stage. This result is not unexpected, because all forward rates are much higher than both reverse ones and rates of losses (see the Table).

Let us discuss in more detail the events occurring in RCs. As was noted above, the primary electron donor is the bacteriochlorophyll dimer with the basic absorption band in the near-IR range at a wavelength of 870 nm (11,494 cm^{-1}). Under natural conditions, the excitation energy comes into RCs from a light-harvesting antenna composed of various bacteriochlorophyll molecules. In the laboratory, isolated RCs are directly excited by light, and an electron located at the bonding orbital of the ground energy level passes to the lower-lying antibonding orbital of the excited singlet level S1. The resulting excited P^* state is highly unstable and exists for no longer than 3 ps. One of the key factors responsible for P^* state instability is the marked shift of electron density toward one (P_B) of the two molecules making up the dimer. The shift occurs within ~ 0.1 ps after the excitation in the form of partial charge separation inside the P dimer. None the less, charge separation actually begins when the electron finally leaves the dimer P. This process lasts roughly 3 ps, i.e., exactly as long as P excitation.

Thus, the electron leaves the excited dimer P within 3 ps (oxidizing it to P^+) and reaches monomeric bacteriochlorophyll molecule B_A (reducing it to B_A^-). This seemingly simple fact has required extensive research over the past 35 years to be established (see Section 5 for details). The electron covers the distance of several angströms between P and B_A molecules as it travels along atomic chains of the protein matrix that fill up the space between P and B_A. There can be several such spatial electron transfer pathways, and their identification remains to be completed (see Section 4). The P^* state thus passes into the primary state with separated charges $P^+B_A^-$ with the rate constant $k_{12} = 1/(3\text{ ps}) = 3.3\times 10^{11}$ s^{-1}. The $P^+B_A^-$ state is, in turn, even more unstable than the P^* state and passes into the $P^+H_A^-$ state for approximately 1 ps ($k_{23} = 1/(1\text{ ps}) = 10^{12}$ s^{-1}), with an electron moving from a B_A molecule to bacteriopheophytin H_A molecule along the respective atomic chain. This transition actually doubles the distance between the separated charges (positive charge on P^+ and negative charge on H_A^-). The $P^+H_A^-$ state is much more stable than the previous $P^+B_A^-$ state, the characteristic lifetime of P^*H_A being about 200 s. The electron uses this time to leave the H_A molecule and pass, with the rate constant $k_{34} = 1/(200\text{ ps}) = 5\times 10^9$ s^{-1}, to a ubiquinone Q_A molecule that is even farther apart from the P dimer than the H_A molecule. This event gives rise to the first metastable state in $P^+Q_A^-$ with a characteristic lifetime of 0.1 s. It is assumed that the primary phase of charge separation in RCs ends with the formation of $P^+Q_A^-$. Thereafter, the electron moves to a secondary quinone Q_B molecule with the participation of the iron atom (see Fig. 1) and leaves the RC to be involved in a long chain of biochemical reactions.

It can be concluded that direct rates of different stages of charge separation vary in the range from 5×10^9 to 10^{12} s^{-1}. These values are not extraordinarily high bearing in mind that many chemical reactions proceed with the same rate.

One key property of RCs is worthy of note: the absence of direct contact between pigment P, B_A, H_A, and Q_A molecules, rigidly fixed in the protein matrix at a certain distance apart from one another. This means that the matrix molecules take part in electron transfer by making up efficient pathways. The speed of the electron movement along these pathways is such that a distance of several angströms between RC pigments is covered by an electron in less than 0.1 ps. The presence of electron pathways accounts for the negligibly small potential barrier for primary charge separation reactions, implying their maximum rate at a given temperature, reorganization energy, and electronic conjugation energy [see formulas (2) and (3)]. On the other hand, the absence of contact between the pigment molecules hampers recombination of separated charges.

It should be emphasized that consideration of primary photosynthetic processes in terms of separate states leads to a serious simplification, even if it is extensively used due to its clearness and simplicity. Many authors have shown (see Refs [1–13]) that the earliest stage of charge separation is characterized by the formation of mixed $P^*(P^+B_A^-)$, $P^+B_A^-(P^+H_A^-)$ states and, possibly, $P^*(P^+B_A^-)(P^+H_A^-)$. The quantum-mechanical mixing results in an electron being able simultaneously to be present (with a certain probability) in each of these states, i.e., belong to P, B_A, and H_A molecules. This might seemingly facilitate and accelerate electron transfer. However, it should be borne in mind that such purely quantum process is an oscillatory one (with a frequency of $\sim (4V^2 + (\Delta E)^2)^{0.5}/\hbar$, where V is the electronic conjugation energy, and ΔE is the difference between energies of states); in other words, it is a reversible process. Both reversibility and state mixing decrease with increasing ΔE. The optimal situation appears to be one in which charge separation ends simultaneously with the termination of the first oscillation half-period.

Let us consider different channels of losses associated with charge separation. To begin with, excitation energy can be lost as a result of $P^* \rightarrow P$ fluorescence. The singlet state S1 for chlorophyll (bacteriochlorophyll) molecules in solutions has an emission lifetime of 10–40 ns, which implies a radiation

decomposition rate of the P^* state: $k_f \sim 10^8$ s^{-1}. For RCs, this time is estimated to vary from a few fractions of a nanosecond to 1 ns, which gives the upper limit of $k_f \sim 10^9$ s^{-1}. In other words, k_f is more than two orders of magnitude lower than k_{12}. The rate constant of the $P^* \rightarrow P$ radiationless transition is much smaller: $k_q \sim 10^6$ s^{-1}. The rate constant of triplet state formation (intercombinational conversion) in RCs is estimated as $k_{tr} \sim 2 \times 10^8$ s^{-1}, which means that total losses of the P^* state proceed with $k_{10} = k_f + k_q + k_{tr} \sim 1.2 \times 10^9$ s^{-1}. Characteristic recombination times of states with separated charges are as follows: ~ 1 ns ($k_{20} \sim 10^9$ s^{-1}) for the $P^+B_A^- \rightarrow PB$ reaction, ~ 15 ns ($k_{30} \sim 7 \times 10^7$ s^{-1}) for the $P^+H_A^- \rightarrow PH$ reaction, and ~ 0.1 s ($k_{40} \sim 10$ s^{-1}) for the $P^+Q_A^- \rightarrow PQ$ reaction.

Reverse reactions are worthy of special consideration. The reverse reaction rate is the product of multiplication of the forward reaction rate by the Boltzmann factor $B = \exp[-\Delta E/(k_B T)]$, where ΔE is the difference between initial and final state energies. At room temperature, one obtains $k_B T \approx 200$ cm^{-1}. For the $P^* \rightarrow P^+B_A^-$ reaction, we find $\Delta E \sim 500$ cm^{-1} and $B = 0.08$. Then, the rate constant of the reverse reaction $P^+B_A^- \rightarrow P^*$ is $k_{21} = 0.08 k_{12} \sim 0.27 \times 10^{11}$ s^{-1}. In an isolated two-level system, the ratio of equilibrium populations of initial and final states equals B. If charge separation ended at the stage of $P^+B_A^-$ formation, approximately 8% of the excited RCs at room temperature would not participate in charge separation. However, the contribution from the next stage, $P^+B_A^- \rightarrow P^+H_A^-$, eliminates the problem due to efficient depopulation of both P^* and $P^+B_A^-$ states. For the $P^+B_A^- \rightarrow P^+H_A^-$ reaction, we find $\Delta E \sim 1500$ cm^{-1} and $B = 5.4 \times 10^{-4}$. Hence, the rate constant of the reverse reaction $P^+H_A^- \rightarrow P^+B_A^-$ is $k_{32} = 5.4 \times 10^{-4} k_{23} = 5.4 \times 10^8$ s^{-1}. For the next reaction, $P^+H_A^- \rightarrow P^+Q_A^-$, the energy difference $\Delta E \sim 3500$ cm^{-1} and $B = 2.4 \times 10^{-8}$. For the reverse reaction, $P^+Q_A^- \rightarrow P^+H_A^-$, one arrives at $k_{43} = 2.4 \times 10^{-8} k_{34} = 120$ s^{-1}. These data suggest that reverse reactions are much slower than direct ones, which prevents repopulation of the P^* state, leading to a rise in fluorescence yield.

As was mentioned in a preceding paragraph, the electron transfer rate in each of the three successive reactions is much higher than that of all other processes responsible for the losses taken together. It is the main cause of the high quantum efficiency of charge separation in RCs, even if absolute electron transfer rates are not enormously high. There is little doubt that all unique properties of RCs are due to their structural organization (see Section 2.2).

All logical links between the structure and functional properties of RCs are far from clarified, despite the obvious success of investigations into their 3D structure by X-ray diffraction analysis. Specifically, active discussions are still underway focused on the surprising association between a drop in temperature to that of liquid helium and a two-to-three-fold rise in the charge separation rate, leading to further enhanced quantum efficiency. Some authors attribute this relationship to the enhanced role of such quantum effects as electron tunneling through the potential barrier [see formulas (2), (3)].

It is worth mentioning once again that the energy efficiency of primary charge separation is much below 100%. Direct losses of energy can be estimated dividing the difference between the energies of initial and final states by the energy of an absorbed light quantum: $\Delta E/(\hbar\omega)$. By way of example, energy losses for the $P^* \rightarrow P^+B_A^-$ reaction are ~ 500 cm$^{-1}/(11{,}494$ cm$^{-1}) = 0.044$, for the $P^+B_A^- \rightarrow P^+H_A^-$ reaction ~ 1500 cm$^{-1}/(11{,}494$ cm$^{-1}) = 0.13$, and for the $P^+H_A^- \rightarrow P^+Q_A^-$ reaction ~ 3500 cm$^{-1}/11{,}494$ cm$^{-1} = 0.3$. The total losses amount to ~ 0.474 or roughly 50%. Absorption of light with a wavelength of 800 nm (the monomeric bacteriochlorophyll $B_{A,B}$ band) or 760 nm (the bacteriopheophytin $H_{A,B}$ band) in RCs gives rise to the respective excited states B^* and H^* that further transmit excitation to the P dimer for 0.1–0.2 ps. In this case, the total losses are somewhat higher: ~ 0.52 and ~ 0.54 for 800-nm and 760-nm light, respectively.

Notice that the consistent lowering of the energy levels in intermediate reaction products are necessary for minimizing the rate constant of reverse reactions. An excess energy is effectively absorbed by the protein environment of RC pigments. An important role in heat removal is also played by carotinoid molecules contained in RCs.

Let us consider a hypothetical situation in which all states depicted in Fig. 2 have an equal energy and thereby evaluate the importance of lowering the energy of states with separated charges. In this case, the activation energy E_a of each reaction markedly increases to one fourth of the respective reorganization energy E_a [see formula (3)]. According to formula (2), rate constants of direct reactions decrease from their maximum values by a factor of $\exp[E_a/(k_B T)]$, which leads to equalization of forward and reverse reaction rates. The use of the known values of $E_r = 650$ cm^{-1}, 1500 cm^{-1}, and 3000 cm^{-1} for the reactions $P^* \rightarrow P^+B_A^-$, $P^+B_A^- \rightarrow P^+H_A^-$, and $P^+H_A^- \rightarrow P^+Q_A^-$, respectively, leads to $k_{12} = k_{21} = 1.5 \times 10^{11}$ s^{-1}, $k_{23} = k_{32} = 1.5 \times 10^{11}$ s^{-1}, and $k_{34} = k_{43} = 1.5 \times 10^8$ s^{-1}; hence, the quantum yield $\Phi_{1-3} = 0.13$ [see formula (6)]. This means that it is impossible to reach a high quantum yield in a system with equal energies of intermediate states.

To recall, charge separation in RCs obeys the second law of thermodynamics [7]. The efficiency of energy storage φ in RCs is defined as $\varphi = 1 - \Delta E/\Delta H$, where ΔE is the energy loss, and $\Delta H = \hbar\omega$ is the increment of internal energy. The difference between the energies of initial (P^*) and final ($P^+Q_A^-$) states enters the expression for the ratio of probabilities to populate these states: $W_{ini}/W_{fin} = \exp[-\Delta E/(k_B T)]$, whence $\Delta E = k_B T \ln(W_{fin}/W_{ini})$. Then, $\varphi = 1 - k_B T \ln(W_{fin}/W_{ini})/(\hbar\omega)$. On the other hand, a change in entropy S in the system is found as $\Delta S = S_{fin} - S_{ini} = k_B \ln(W_{fin}/W_{ini})$. Substituting the expression for ΔS into the relationship for φ yields $\varphi = 1 - T\Delta S/(\hbar\omega) = (\Delta H - T\Delta S)/\Delta H$. The last expression coincides with the expression for the efficiency of a thermal machine in classical thermodynamics.

3. Coherent and incoherent electron transfer along the B-branch

3.1 B-branch activation by site-directed mutagenesis

Because the B-branch in native RCs is practically inactive, electron transport along this chain is explored after its artificial activation by site-directed mutagenesis (see paper [146] for a review of earlier publications).

RCs of *Rba. sphaeroides* and *Rba. capsulatus* possess similar electron transfer rates between different states, but some exiting structural distinctions make activation of the B-branch in RCs of *Rba. sphaeroides* more difficult than in *Rba. capsulatus* [147, 148]. The quantum yield of $P^+H_B^-$ over

30% is possible to reach by using β-mutations to substitute bacteriochlorophyll BChl for H_A and thereby to raise the $P^+\beta^-$ energy level compared with that of the $P^+H_A^-$ and slow down electron transfer along the A-branch [147–150]. Small changes in the energy levels of $P^+H_A^-$ and $P^+H_B^-$ have no effect on B-transfer efficiency [147].

The rate constant of the $P^+H_B^- \rightarrow P^+Q_B^-$ reaction is commensurate with that of the $P^+Q_B^-$ recombination and much lower than the $P^+H_A^- \rightarrow P^+Q_A^-$ reaction rate constant [149, 150]. Factors determining the difference between these rates are differences in the energies of reorganization of these reactions, the mutual position of the energy levels of states, and the magnitude of electronic conjugation [149, 151]. Differences in electronic conjugation are due to the different character of quinone interactions with the nearest amino acid residues, such as Trp M252 in RCs of *Rba. sphaeroides*, Trp M250 near Q_A, and Phe L216 near Q_B in RCs from *Rba. capsulatus*.

Inhibition of electron transfer along the A-branch makes it possible in the B-branch up to Q_B [152]. Such a blockade is realized by removing Q_A from the RC [55, 151, 153, 154]. The Q_B^- yield upon inhibition of the A-transfer depends on additionally introduced mutations [155–157]. EL212A and DL213A mutations in RCs of *Rba. sphaeroides* bring in less polar residues that increase the Q_B^- yield in the B-transfer due to a change in both the redox-potential and the reorganization energy [155]. Results of calculations suggest that $P^+Q_B^-$ recombination has a much higher reorganization energy than the $P^+Q_A^-$ reaction. This discrepancy accounts for the more than 10-fold difference between the rates of these reactions [158].

Calculations by molecular dynamics method show that the $P^+B_B^-$ energy level in RCs of *Rba. sphaeroides* is ~ 4 kcal mol^{-1} higher than the P^* level, which is one of the main causes of the extremely low activity of the B-branch [93, 159, 160]. The difference between theoretical energy levels of $P^+B_B^-$ and $P^+B_A^-$ is partly due to the presence of Tyr M210 in RCs of *Rba. sphaeroides* (Tyr M208 in RCs of *Blc. viridis* and *Rba. capsulatus*) that stabilizes B_A^- [93, 161]. The role of Tyr M210 is considered in greater detail in Section 4.

Phe 181, the homologous residue in the B-branch, appears to be incapable of stabilizing B_B^- in the same manner. The replacement of Tyr M210 by a different amino acid residue slows down charge separation by increasing the activation energy of the reaction [64, 65, 114, 162–164]. It has been shown that the $P^+H_B^-$ state with a quantum yield of 15–30% forms in RCs of the YM208F/FL181Y mutant of *Rba. capsulatus* [49, 50]. Similar state was not found in the analogous mutant of *Rba. sphaeroides* [163].

A large number of mutants have been prepared to lower the $P^+B_B^-$ energy level and thereby activate electron transfer along the B-branch [49, 50, 54–56, 74, 75, 145–148, 165–172]. The $P^+H_B^-$ state with a quantum yield of 70% was obtained by inhibiting electron transfer along the A-branch based on the exchange of amino acid residues in D-helices between L- and M-subunits, followed by the introduction of FL181Y, HM195F, and HL168F mutations lowering the $P^+B_B^-$ energy level [172]. These data show that the position of the $P^+B_A^-$ energy level below the P^* level and the position of the $P^+B_B^-$ level above the P^* level in native RCs contribute to the asymmetry of A- and B-branches with respect to electron transfer.

It has been demonstrated theoretically that the matrix element of electronic conjugation (V) between P^* and B_A is much larger than that for P^* and B_B. It may be one more cause of B-branch inactivity [173–176]. If V is much smaller than the difference between energy levels of the donor and the reaction product, the electron transfer rate is proportional to V^2 and exponentially decreases with increasing distance between the donor and the acceptor [177–182]. If V is commensurate with the difference between energy levels of the donor and the product, the electron transfer rate is virtually independent of V [140, 141].

It has been argued that fluctuations of the distance between an electron donor P^* and acceptor, e.g., B_A and B_B, markedly reduce the difference between V values [178]. The distinction between the dielectric properties of protein in A- and B-branches can be one more cause of B-branch inactivity [183]. However, calculations show that the reorganization energies of reactions $P^* \rightarrow P^+B_A^-$ and $P^* \rightarrow P^+B_B^-$, as well as the contributions of induced dipoles to the free energies of $P^+B_A^-$ and $P^+B_B^-$, differ but insignificantly [93].

Some theoretical work deals with the dependence of electronic conjugation V on the door–acceptor distance in a homogeneous protein environment [184–186]. This dependence is roughly exponential. The spatial symmetry of the two RC branches suggests approximate comparability of V values for different stages of electron transfer along these branches, as evidenced by investigations using mutants with activated B-transfer [56, 187]. Nonetheless, a comparison of the difference between $P^* \rightarrow P^+H_A^-$ and $P^* \rightarrow P^+H_B^-$ reaction rates with that between $P^+H_A^-$ and $P^+H_B^-$ free energy levels shows that the slow electron transfer along the B-branch in mutant RCs is due not only to different energy characteristics but also to different V values [49, 188].

Calculations of electrostatic potentials for RCs of *Blc. viridis* give evidence that the A-branch possesses a much higher positive potential than the B-branch; this is one more cause accounting for the predominantly A-branch electron transfer [94]. They also show that the orientation of the 13^2-ether group in BChl has a strong influence on electrostatic potentials [189]. The calculations confirm the well-known experimental fact that potential E_m for the primary electron donor of the II P680 photosystem is much higher than for the P in bacterial RCs [190]. Simulations by the molecular dynamics method also give potential values consistent with the prevalent electron transfer along the A-branch. Experimental estimations of electric field strengths inside RCs by Stark spectroscopy give values on the order of 10^6 V cm^{-1} near P [191]. A roughly 10% change in this value after removal of the carotinoid molecule from the RC does not alter the electron transfer rate [192].

A comparative study of electron transfer in RCs of A- and B-side heterodimeric mutants revealed the difference in electronic conjugation between P and H_A, on the one hand, and between P and H_B, on the other hand [188]. A combination of various mutations makes it possible to achieve a similar position of the energy levels of primary states with separated charges in A- and B-side heterodimeric mutants. The accompanying four-fold increase in electron transfer yield in the B-branch of the B-side heterodimeric mutant over that in the A-side mutant can be explained by the difference in electronic conjugation of P and $H_{A,B}$. Electronic conjugation in the A-branch is stronger, which is one of the factors explaining why electron transfer occurs predominantly along this branch.

It has been shown that RC excitation by blue light gives rise to the appearance of $B_B^+H_B^-$ state in the Sore absorption

band of the P dimer that degrades within a few picoseconds at 293 K; it exists much longer at low temperatures [103, 193]. It was concluded based on these findings that the B-branch plays an important role in rapid quenching of the excess of exciting energy with the participation of the carotinoid molecule located close to the B-branch [71, 72, 103].

It follows from the foregoing that site-directed mutagenesis provides a powerful tool for activation of electron transfer along the B-branch. The transfer of an electron to H_B is limited by the high $P^+B_B^-$ level energy and weak electronic conjugation in H_B and P^*. The further electron transfer to Q_B occurs only after blockading the A-transfer. The Q_B^- yield is limited mostly by the high energy of reaction reorganization responsible for Q_B^- formation.

3.2 Coherent electron transfer along the B-branch

Coherent electron transfer along the B-branch is rather poorly known. It has been studied in association with primary charge separation in the B-branch of the HM182L mutant and in RCs of *Cfx. aurantiacus* [195]. In these RCs, electrons may be transferred from P^* to the B-branch. The HM182L mutation results in the replacement of a bacteriochlorophyll B_B molecule into the B-branch of RCs of *Rba. sphaeroides* by a bacteriopheophytin Φ_B molecule [74]. In this mutant, the $P^+\Phi_B^-$ energy level is ~ 0.16 eV lower than the P^* level, which accounts for incoherent transfer of an electron onto Φ_B with a small quantum yield of $\sim 12\%$ at 77 K and characteristic time of ~ 8 ps [56, 187]. The $P^+\Phi_B^-$ state recombines to the ground state with a time constant of ~ 200 ps at room and cryogenic temperatures [56, 74, 187].

Further charge separation in RCs containing Φ_B instead of B_B with the formation of the $P^+H_B^-$ state is arrested, because the free energy level of $P^+\Phi_B^-$ resides below that of $P^+H_B^-$ [56, 187]. The B-branch in RCs of *Cfx. aurantiacus* also contains a Φ_B molecule in position B_B, which makes these RCs similar to RCs of the HM182L mutant [18, 19]. Estimates of the $P^+\Phi_B^-$ energy level in RCs of *Cfx. aurantiacus* give evidence that it lies near or even lower than the P^* level, which suggests that electron transfer over the B-branch is theoretically possible in these RCs. The authors of Ref. [97] considered low-temperature fluorescence kinetics in RCs of *Cfx. aurantiacus* with reduced Q_A and concluded that fast reversible electron transfer between $P^*$and BPheo is possible over the B-branch. However, results of differential absorption spectroscopy in the Q_x band of BPheo molecules and the close-to-unity quantum yield of primary charge separation in RCs of *Cfx. aurantiacus* indicate predominant electron transfer along the A-branch [91, 92, 98].

RCs of the HM182L mutant exhibit a weak 1020-nm absorption band of B_A^-, which makes it possible to study the earliest stage of charge separation in the A-branch [194]. Formation of the $P^+B_A^-$ state in the HM182L mutant in response to femtosecond excitation takes place qualitatively as it is in RCs of *Rba. sphaeroides* R-26; in other words, it is accompanied by pronounced oscillations both in the stimulated P^* emission band and in the B_A^- absorption band. These are in-phase oscillations. Their first most intense maximum occurs with a lag of ~ 120 fs from the onset of excitation. The HM182L mutant also undergoes mild dynamic bleaching of the Φ_B absorption band at 785 nm. This bleaching, observed only with a delay in the range from 0 to 80 fs with respect to the instant of excitation, suggests the reversibility of electron transfer to the B-branch with the formation of the $P^+\Phi_B^-$ state. The ΔA kinetics of the Φ_B absorption band at 785 nm have the form of a single peak with the maximum at ≈ 40 fs, whereas the first peak of oscillations in the B_A^- and P^* bands appears ≈ 80 fs later (Fig. 3). Notice that there is still no B_A^- absorption band in association with a ~ 40-fs delay.

Damped oscillations in the 748- and 785-nm absorption bands of Φ_B were detected in RCs of *Cfx. aurantiacus* upon

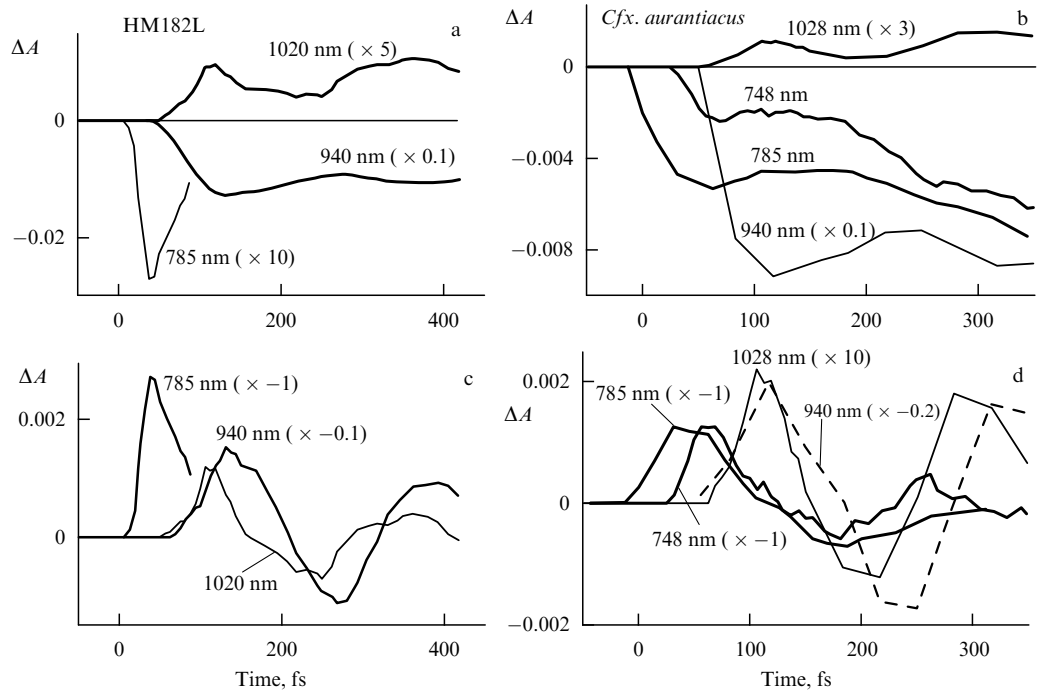

Figure 3. The ΔA kinetics (a, b) and their oscillating component (c, d) of the Φ_B absorption bands at 785 and 748 nm, and B_A^- absorption bands at 1020–1028 nm and stimulated P^* emission bands at 940 nm in RCs of the HM182L mutant of *Rba. sphaeroides* (a, c) and in RCs of *Cfx. aurantiacus* (b, d) [194, 195]. RCs were excited at 90 K by 20-fs pulses with a wavelength of 870 nm.

femtosecond excitation [195] (see Fig. 3). Bleaching of the 785-nm band begins with a very short delay ($\approx$ 10 fs) after excitation origin and continues up to appearing the first maximum with a lag of $\approx$ 25 fs. Bleaching of the 748-nm band begins with a somewhat longer delay (30 fs) and reaches the first maximum with a lag of about 60 fs. Thereafter, oscillations develop synchronously in both bands with a mean period of 200–220 fs. A Fourier analysis of oscillations revealed characteristic frequencies of 79 and 108 cm^{-1} in 785-nm band oscillations, and 73 and 154 cm^{-1} in 748-nm band oscillations. Synchronous oscillations of stimulated P^* emission at 940 nm and B_A^- absorption at 1028 nm in RCs of *Cfx. aurantiacus* develop much later. Their first maximum appears with a lag of $\sim$ 100 fs; they are absent earlier than 50 fs after the instant of excitation.

Thus, electron transfer over the B-branch of the RCs of HM182L mutant and RCs of *Cfx. aurantiacus* is accompanied by oscillations in the state with separated charges. These oscillations begin a few dozen femtoseconds before oscillations accompanying electron transfer along the A-branch. Oscillations in the B-branch of HM182L RCs have the form of a single peak, while oscillations in RCs of *Cfx. aurantiacus* rapidly damp out. The available data provide a deeper insight into coherent processes accompanying primary charge separation in RCs undergoing femtosecond excitation. Excitation of P by 18–20-fs pulses in a wide wavelength range gives rise to a nuclear wave packet that begins oscillatory motion over the P^* surface along two independent coordinates corresponding to $P^* \rightarrow P^+B_A^-$ and $P^* \rightarrow P^+\Phi_B^-$ reactions. Immediately after its formation, the wave packet is localized at the short-wavelength slope of the P^* surface and emits light with a wavelength of $\sim$ 900 nm. The fact of beginning the oscillations in the absorption band of the primary electron acceptor in the B-branch immediately after excitation suggests close proximity of the intersection site of P^* and $P^+\Phi_B^-$ potential surfaces to the region where the wave packet forms. The time course of these oscillations gives evidence of reversible electron transfer along the B-branch under the action of the wave packet.

The wave packet reaches the area of intersection between P^* and $P^+B_A^-$ surfaces at the long-wavelength slope of the P^* curve with a lag of $\approx$ 100–120 fs relative to the onset of excitation. In this region, the emission from the wave packet occurs at a wavelength of 930–940 nm. The appearance of the wave packet in the vicinity of the intersection between the P^* and $P^+B_A^-$ surfaces gives rise to oscillations in the B_A^- absorption band in phase with oscillations of P* emission at 940 nm. After the wave packet reflects from the intersection region and moves away in the opposite direction, absorption in the B_A^- band sharply decreases, which suggests the reversibility of the coherent $P^* \rightarrow P^+B_A^-$ reaction and the absence of stabilization of separated charges with such a delay.

Thus, coherent components of electron transfer reactions along the A- and B-branches are separated in time, with the B-transfer starting 60–80 fs before the A-transfer. This suggests a difference in optimal nuclear configurations for electron transfer along the two branches. After a $\approx$ 200–250-fs delay relative to the excitation instant of time, the wave packet again finds itself at the left slope of the P^* surface near the P^* and $P^+\Phi_B^-$ intersection region. In RCs of *Cfx. aurantiacus*, this gives rise to the second peak of oscillations in the Φ_B^- absorption band. Similar peaks are absent in the HM182L mutant, which indicates a drop in the wave packet energy by this time that becomes too low to contribute to overcoming the potential barrier. After a $\approx$ 350-fs delay, the wave packet can be observed again at the right slope of the P^* surface near the P^*–$P^+B_A^-$ intersection site, which causes the second maximum in product oscillations at 1020 nm and P* emission at a wavelength of 940 nm. The wave packet rapidly smears out as it moves due to dephasing and dissipation; therefore, only a few oscillation periods can be recorded.

To sum up, the femtosecond excitation of RCs in *Cfx. aurantiacus* and *Rba. sphaeroides* with M182 mutation is associated with the back electron transfer from P^* to the low-active B-branch, which totally depends on the movements of the nuclear wave packet. The transfer starts very soon after photoexcitation of the P dimer and 60–80 fs before the onset of analogous transfer along the A-branch. Electron transfer over the B-branch occurs only in the presence of a wave packet at the short-wavelength slope of the potential P^* surface close to its intersection with the potential surface of the primary state with separated charges in the B-branch.

4. Influence of environment on charge separation

4.1 Consequences of point changes in pigment environment

Site-directed mutagenesis allowing the substitution of amino acid residues coordinating cofactors and cofactors themselves is widely used to elucidate the influence of environment on electron transfer in RCs.

For example, the replacement of one of the ligands of the central magnesium atom in P in a heterodimeric mutant results in the replacement of the one of two BChl molecules in P by a Pheo molecule. This effect is produced by the substitution of leucine for His L173 and His M202 in *Rba. sphaeroides* and the substitution of leucine for His L173 and His M200 in *Rba. capsulatus* [38, 58, 101, 106, 196, 197]. Such a substitution is possible for both BChl molecules in P, but their simultaneous substitution by BPheo molecules makes the P dimer unstable.

Another example is given by the HM182L mutant of *Rba. sphaeroides*, whose RC contains BPheo instead of B_B; the analogous mutation in the A-part fails to produce this effect [74, 75]. Conversely, in the LM214H mutant of *Rba. sphaeroides* (LM212H in *Rba. capsulatus*), H_A is replaced by bacteriochlorophyll [198]. The appearance of His near H_B in the LL185H mutant of *Rba. sphaeroides* results in the replacement of H_B by bacteriochlorophyll [199]. A change of ligands of the iron atom in the HM266C mutant of *Rba. sphaeroides* causes the replacement of Fe by a zinc atom [200].

Certain of RC cofactors can be removed from the structure of RCs, as exemplified by the R-26 strain of *Rba. sphaeroides*, whose RCs do not contain a carotinoid molecule. Quinones can be removed from RCs by treatment with detergents. Biosynthesis of Q_A can be inhibited by the replacement of amino acid residues forming the Q_A-binding pocket. Such an inhibition is realized by the removal of Trp M252 in *Rba. sphaeroides* (M250 in *Rba. capsulatus*), which is in van der Waals contact with Q_A, or by the substitution of Trp for a smaller residue in the AM260W mutant of *Rba. sphaeroides* [153]. Certain mutations near P result in the loss of functionally active P in RCs, as exemplified by VL157R, HL153E, HL153L, HL153Q, HL153Y, HL137E, and HM202E mutants of *Rba. sphaeroides* [75, 201, 202]. One of the consequences of major changes in the D_{LL}-mutant is the

loss of H_A, resulting in the replacement of the D-transmembrane sequence from the M-subunit (M192–M217 in *Rba. capsulatus*) by a symmetric segment from the L-subunit (L165–L190 in *Rba. capsulatus*) [53, 203]. The analogous mutation AM149W in *Rba. sphaeroides* causes the loss of H_B [199]. The loss of BChl in P occurs in the IL177H mutant of *Rba. sphaeroides* as a result of structural and electrostatic changes to the residue residing between B_B and P [204].

Certain mutations are associated with marked changes in the midpoint redox-potential E_m of the P/P^+ couple, which is about 500 mV in native RCs of *Rba. sphaeroides*. Thus, it increases by 130 mV in the heterodimeric mutant [197]. Most mutations affecting P lead to moderate changes in E_m of P/P^+ — by the value of $\leqslant 50$ mV [205]. Adding the H-bond between P and its environment enhances E_m by the value of order 60–120 mV, while elimination of an existing H-bond decreases E_m by ≈ 80 mV [206–210]. Combining various mutations influencing the number of H-bonds in the dimer allows E_m to be changed in a wide range from -80 to 260 mV, compared with the initial value [211].

As a rule, a rise in the number of H-bonds of the P dimer slows down charge separation in RCs. The addition of an H-bond to B does not cause appreciable changes in a primary charge separation [212]. The presence of hydrogen bonds linking $H_{A,B}$ to its environment facilitates their recovery, which affects the electron transfer rate. The H-bond between the H_A 13^1-ketogroup and the residue Glu L104 is present in native RCs of *Rba. sphaeroides* and *Rba. capsulatus*, while the analogous bond with H_B is created in the VM131D mutant of *Rba. sphaeroides* and VM133D mutant of *Rba. capsulatus* [58, 147, 213]. Introducing or removing the ionizable residues at the L135, L155, L164, L170, L247, and M199 locations in RCs of *Rba. sphaeroides* decreases E_m of the dimer by $\leqslant 60$ mV in the case of a negative charge, and increases it by $\leqslant 50$ mV in the case of a positive charge [214–216]. The influence of introduced charges on E_m decreases due to shielding of charge interactions by the protein environment.

The $B_{A,B}$ energies change as a result of the YM210F mutations in *Rba. sphaeroides* (YM208F mutations in *Rba. capsulatus*) and the FL181Y mutations; these changes are recorded either from variations of the electron transfer rate [64, 66, 162] or by Stark spectroscopy [217]. Calculations show that these mutations are responsible for the changes in electrostatic fields near $B_{A,B}$, which influences the energy levels of $P^+B^-_{A,B}$ states [94, 218].

The results of measurements and calculations of electron-spin density of an unpaired electron in RCs with oxidized P^+ demonstrate its marked shift from P_M toward P_L [28–30]. The addition of an H-bond to P_M makes this shift even more asymmetric due to a reduced P_M energy level and greater difference between the energies of P_L and P_M molecular orbitals. In contrast, the addition of an H-bond to P_L makes the electron-spin density distribution between P_L and P_M more symmetric. Taking account of vibrational states in theoretical calculations allows estimating the influence of H-bonds with P_L and P_m on the optical absorption spectra of RCs [30, 219, 220].

Certain mutations have a negligible effect on the energy characteristics of primary reactions, whereas others induce serious changes in the RC structure. For example, the replacement of the residue His M202 coordinating P by Leu in RCs of *Rba. sphaeroides* results in appearing a heterodimer, whereas the substitution of the same His by Glu does not really change the RC properties due to the introduction of water as a ligand instead of His [221]. Substitution of His L153 coordinating B_A by a smaller residue (serine (Ser) or glycine in *Rba. sphaeroides*, threonine (Thr) or Ser in *Rba. capsulatus*, or Cys in *Blc. viridis*) has almost no effect on RC properties, whereas the replacement of the same His by Leu alters pigment composition in RCs [75, 222–225].

H-bonding between intermediate electron acceptors and the protein environment also influences the energy characteristics of electron transfer reaction. For example, elimination of the H-bond between Glx L104 (Glx is glutamic acid or glutamine residue) and the H_A 13^1-ketogroup in RCs of *Rba. sphaeroides* and *Rba. capsulatus* slightly decreases the charge separation rate, in agreement with the reduced difference between free energies of the P^* and $P^+H^-_A$ levels [226].

Certain mutations may be utilized to create RCs with a secondary electron donor, such as tyrosine or the Mn atom. Such a modification likens these mutant RCs with RCs of the photosystem II. Thus, the addition of H-bonds to the P dimer increases its potential and offers the possibility of electron transfer to P^+ from tyrosine inserted at a location analogous to that of Y_Z tyrosine in RCs of photosystem II [227–230]. The analogous electron transfer to P^+ occurs from the Mn atom near P, introduced into the RC as a result of a series of mutations [231, 232].

Results of numerous genetic manipulations confirm a high resistance of bacterial RCs to various mutations. Photoreduction of H_A in RCs of many mutants having a complete set of pigments results in a high quantum yield, despite the enhanced $P^+B^-_A$ level and the related decrease in the charge separation rate [53, 145, 170, 203]. Mutations that change the sign of the charge on Arg L135 and M164 molecules, i.e., the ionizable residues closest to P, have almost no effect on the $P^+H^-_A$ state kinetics [233]. Mutations changing the number of hydrogen bonds between electron carriers and protein moderately affect charge separation in RCs as well [44, 67, 207]. Only a combination of several mutations is able to appreciably activate electron transfer along the B-branch [49, 50, 145, 170, 172, 234]. Even mutations slowing down primary charge separation in the A-branch by a factor of 10 or more due to the markedly enhanced $P^+B^-_A$ level cannot completely block electron transfer along the A-branch at low temperatures [65, 67].

Generally speaking, organisms with different types of reaction centers, each occupying its specific natural niche, are equally successful in terms of survival. Variation of the characteristic time of the primary stage of charge separation from several picoseconds to a few fractions of a picosecond does not affect subsequent biochemical stages of photosynthesis in natural cultures. Only some mutant cultures obtained artificially by a combination of various mutations are suitable for observing the correlation between decelerations of primary charge separation (several dozen times) and biomass growth. As a rule, it is much more difficult to grow such mutant cultures.

4.2 Role of tyrosine M210 in stabilization of separated charges

The spatial structure of RCs of *Rba. sphaeroides* is such that oxygen in tyrosine M210 localizes symmetrically between P_A and $B_A \approx 5$ Å apart from both the carbon in C-N(IV) in P_A and nitrogen N(II) in B_A (see Protein Data Bank (PDB), file 1AIJ) (Fig. 4). It is well known that substituting Tyr M210 by triptophane in the YM210W mutant or by leucine in the YM 210L mutant results in a very strong increase of the P^* lifetime

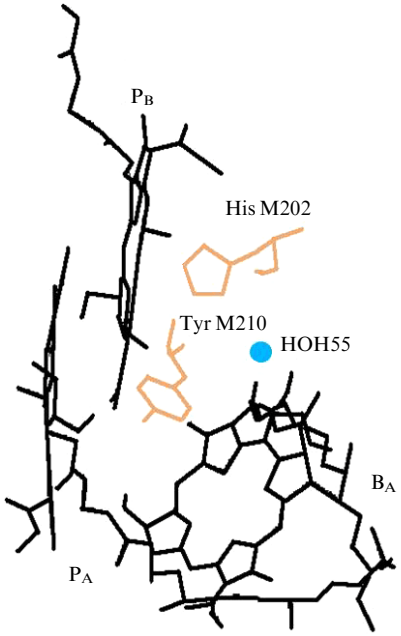

Figure 4. (Color online). A fragment of the RC spatial structure in *Rba. sphaeroides* (PDB, file 1AIJ). BChl P_A and P_B molecules, monomeric BChl B_A (black lines), His M202, Tyr M210 (light brown lines), and HOH55 (blue circle) molecules are shown. Oxygen of Tyr M202 localizes symmetrically between P_A and B_A approximately 5 Å apart from carbon of C-N(IV) in P_A and nitrogen N(II) in B_A. HOH55 water is separated from the oxygen of the 13^1-ketocarbonyl group in B_A and the nitrogen atom in His M202 by the distance of the H-bond formation.

by a factor of several dozens [65, 66, 112, 114, 133, 164]. Because this fact cannot be a consequence of the relatively small increase in P/P^+ redox-potential in these mutants (by 55 mV in YM210W, and 30 mV in YM210L) [114], a different mechanism behind the influence of Tyr M210 on charge separation in RCs should be postulated. For comparison, only a much greater (by 260 mV) increase in the midpoint P/P^+ redox-potential in the triple mutant LL131H/LM160H/FM197H as against the native *Rba. sphaeroides* produces a similarly marked slow-down in charge separation rate in RCs [235]. X-ray diffraction analysis of RC crystals in the YM210W mutant revealed the absence of appreciable changes in the RC structure outside the mutation site [236]. The triptophane present in YM210W causes a slight tilt of the B_A macrocycle by acting largely on the position of pyrrole cycles II and III [236]. The mechanism of Tyr M210 action on charge separation has been investigated spectroscopically with a temporal resolution of 20 fs in several tyrosine mutants of RCs from *Rba. sphaeroides* [237–239].

The ΔA kinetics of YM210W mutant at 935–940 nm demonstrates very slow attenuation of stimulated P^* emission in a picosecond range, accompanied by quite apparent intricately shaped oscillations [237] (Fig. 5). Data obtained earlier suggest that the P* lifetime in YM210W(L) mutants is tens of times that in native RCs. The oscillation amplitude of P^* stimulated emission in RCs of the mutants is close to that of analogous oscillations in native RCs. Unlike oscillations in native RCs, stimulated P^* emission oscillations in mutant RCs last ≈ 1.5 ps (≈ 0.5 ps in native RCs), which makes it possible to observe up to 7 peaks. The first and most intense of them occurs with a ≈ 120-fs delay after excitation. The Fourier spectrum of stimulated P^* emission oscillations in the YM210W mutant exhibits a wide dominant band with a complicated shape and with the center at a frequency of ≈ 150 cm^{-1}, which corresponds to a fundamental oscillation period of ≈ 230 fs. The YM210L/FM197Y mutant spectrum is characterized by a low-frequency shift of the baseband in the Fourier spectrum of stimulated P^* emission oscillations

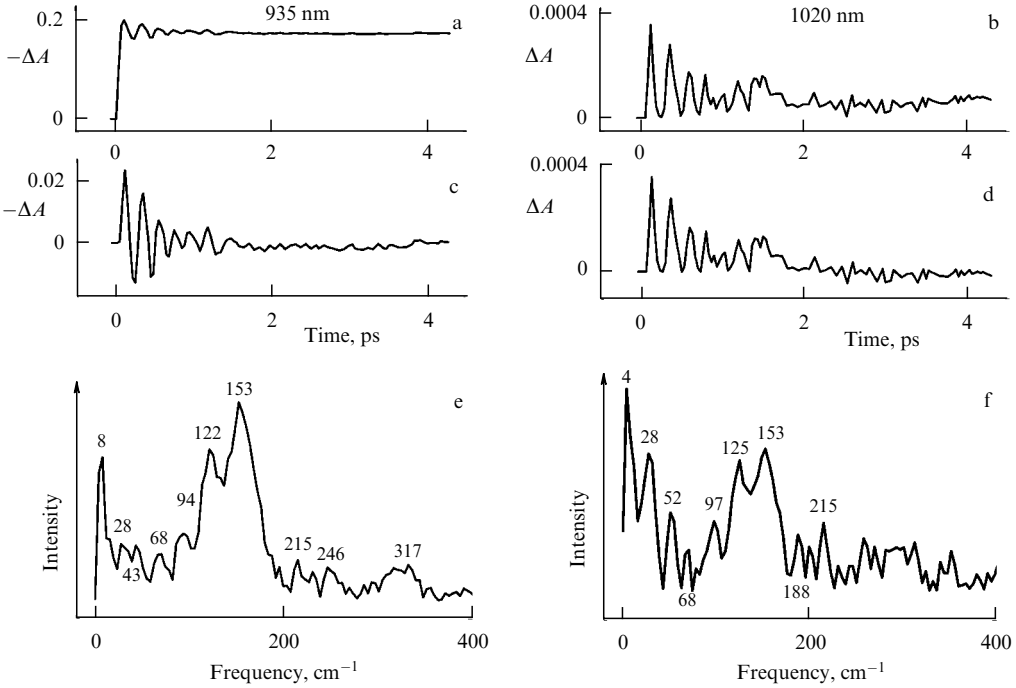

Figure 5. The ΔA kinetics (a, b), their oscillating component (c, d), and Fourier transform spectrum of the oscillating component (e, f) of the stimulated P^* emission band at 935 nm (a, c, e) and the B_A^- absorption band at 1020 nm (b, d, f) in RCs of the YM210W mutant of *Rba. sphaeroides* [237]. RCs were excited at 90 K by 20-femtosecond pulses with a wavelength of 870 nm. Numerals in figures e and f denote frequencies of Fourier spectrum peaks.

from 150 to 100 cm^{-1}, suggesting a rise in the effective mass of some part of concertedly oscillating (due to femtosecond excitation) molecular groups coupled to new ones through hydrogen bonding [238]. In the YM210L/HL168L mutant, the Fourier spectrum of stimulated P^* emission oscillations contains two basic overlapping bands at 117 and 152 cm^{-1}; these oscillations decay somewhat faster than in other aforementioned mutants [239].

The spectra of all these mutants exhibit a very weak B_A^- anion absorption band at 1020 nm. Its appearance unambiguously indicates the participation of B_A in primary electron transfer from P^* in the above-mentioned mutants. The same conclusion follows from the results of femtosecond spectroscopy of the YM210W mutant in the medium IR range [240]. The shape and the spectral position of this band are identical with those of the respective band in native RCs of *Rba. sphaeroides* R-26. The ΔA kinetics of the above mutants at 1020 nm suggests the practically total absence of a stable $P^+B_A^-$ state in RCs of YM210W (see Fig. 5) and YM210L/FM197Y mutants and very weak stabilization of the $P^+B_A^-$ state (in the form of a constant component in kinetics) in RCs of YM210L/HL168L mutant [238, 239]. The RCs of these mutants exhibit oscillations of the B_A^- absorption band as a whole, without a change in its shape and position, similar to analogous oscillations in native RCs. The above oscillations are roughly synchronous with those of stimulated P^* emission. The character of oscillations in the 1020-nm band suggests an almost completely reversible electron transport between P^* and B_A caused by the motion of the nuclear wave packet near the intersection site of P^* and $P^+B_A^-$ potential surfaces. The oscillation amplitude of the B_A^- absorption band in mutant RCs is several times smaller than that in native and pheophytin-modified RCs. Oscillations of the mutants in the B_A^- absorption band stop approximately 1.5 ps after excitation. B_A^- band oscillations similar to P^* oscillations have up to 7 peaks. The Fourier spectrum of oscillations of the above mutants in the B_A^- band contains bands characteristic of analogous P^* oscillations, as well as a few narrow low-frequency bands in the 10–70-cm^{-1} range, with a very conspicuous 28–33-cm^{-1} band among them.

An analysis of experimental data allows concluding that the presence of Tyr M210 in RCs is necessary to ensure the stabilization of separated charges in the $P^+B_A^-$ state. Irreversible electron transfer from P^* to B_A is practically absent in mutants lacking Tyr M210, and the P^* lifetime in them is tens of times that in native RCs containing Tyr M210. Reversible femtosecond electron transfer from P^* to B_A in mutants without Tyr M210 suggests the absence of stabilization of the primary $P^+B_A^-$ state with separated charges.

The two aspects of $P^+B_A^-$ stabilization in RCs can be distinguished. First, an electron can be transferred from P^* to a higher vibrational level of the $P^+B_A^-$ potential energy surface with subsequent vibrational relaxation to a lower lying level. Effective stabilization of $P^+B_A^-$ through vibrational relaxation is possible if the potential surface of $P^+B_A^-$ lies much lower than that of P^*. The characteristic time of vibrational relaxation restricts the rate of charge separation between P^* and B_A. In the YM210L/HL168L double mutant molecule, the second mutation decreases the redox-potential of the P^+/P couple by 123 mV [205]. It may lower the $P^+B_A^-$ level relative to that of P^* and enhance the role of vibrational relaxation in the course of the $P^+B_A^-$ state stabilization. The absence of appreciable stabilization of the $P^+B_A^-$ state in the YM210L/HL168L double mutant molecule confirms the important role played by Tyr M210 in this process and suggests it has a different mechanism. The presence of Tyr M197 in the YM210L/FM197Y double mutant molecule does not change the situation, as evidenced by the absence of $P^+B_A^-$ state stabilization in this mutant.

Second, stabilization of the $P^+B_A^-$ state can result from reorientation of the surrounding polar groups under the effect of separated P^+ and B_A^- charges. The nuclear configuration in native RCs can be altered by reorientation of the $O^{\delta-}H^{\delta+}$ type polar groups in Tyr M210. The travel of $H^{\delta+}$ toward B_A^- reduces the energy of $P^+B_A^-$ relative to P^* energy and thereby stabilizes the $P^+B_A^-$ state. $H^{\delta+}$ of the OH group in Tyr M210 may occupy two characteristic positions with respect to P_A and B_A. In one of them, the $O^{\delta-}H^{\delta+}$ dipole of tyrosine M210 is perpendicular to the line connecting the carbon C-N(IV) P_A and nitrogen N(II) B_A, which are the nearest neighbors of Tyr M210 and have maximum positive and negative charges, respectively, in the $P^+B_A^-$ state [241]. This position occurs in the PB_A or P^*B_A neutral state. In the second position, $H^{\delta+}$ of the OH group in Tyr M210 localizes on the line connecting oxygen $O^{\delta-}$ of the OH group in Tyr M210 and nitrogen N(II) B_A. This position is realized when $P^+B_A^-$ is stabilized due to the motion of $H^{\delta+}$ toward B_A under the effect of attraction to B_A^- and repulsion from P_A^+. An estimation of electrostatic interaction energy gives a difference of about 900 cm^{-1} between the two positions. Experimental values of the energy difference between P^* and $P^+B_A^-$ for the stable $P^+B_A^-$ state in pheophytin-modified RCs are about 550 cm^{-1} (see Section 5).

It follows from the foregoing that the energy spent to reorient the OH group in Tyr M210 is sufficient to stabilize the $P^+B_A^-$ state. Importantly, the attraction and repulsion of $H^{\delta+}$ by B_A^- and P_A^+ charges, respectively, take place only in the case of $P^+B_A^-$ formation but not in the neutral P^*B state. The experimentally observed growth in stabilization time with increasing temperature is consistent with the proposed mechanism, since the interaction between $H^{\delta+}$ of the OH group in Tyr M210 and phonons of the environment can induce some additional movements of $H^{\delta+}$, leading to an increase in stabilization time.

RCs from *Cfx. aurantiacus* have no Tyr M210 mutant molecule but contain Tyr M195 [77] located between P and B_A that may be responsible for $P^+B_A^-$ stabilization in these RCs. Stabilization of $P^+B_A^-$ in RCs of *Cfx. aurantiacus* at 90 K takes more time ($\approx$ 5 ps) than in RCs from *Rba. sphaeroides* R-26 ($\approx$ 1.5 ps) [195], in agreement with the asymmetric position of Tyr M195 relative to P_A and B_A (in contrast to that of Tyr M210).

The markedly decreased amplitude of oscillations of the $P^+B_A^-$ state population in mutant RCs compared with native RCs means that a substantial part of the wave packet does not reach the intersection site of P^* and $P^+B_A^-$ surfaces in mutant RCs. Such a situation takes place if the intersection site lies high enough on the energy scale, i.e., when the $P^+B_A^-$ surface is above the P^* surface, and the activation energy of the $P^* \rightarrow P^+B_A^-$ reaction is comparable with that of the wave packet. The relatively slow decay of oscillations in mutant molecules containing no Tyr M210 is a consequence of the absence of incoherent changes in the nuclear configuration during reverse movements of the wave packet over the P^* surface and its periodic appearance near the intersection site of the P^* and $P^+B_A^-$ surfaces.

Experimental data on tyrosine mutant RCs from *Rba. sphaeroides* are consistent with the results of calculations by the molecular dynamics method, showing that the presence of

Tyr M210 mutant molecules lowers the energy level of a perfectly stabilized $P^+B_A^-$ state by more than 1000 cm^{-1} due to the collective action of two mechanisms involving the static charge redistribution in the adjacent region and the dynamic effect of reorientation of the polar OH group in Tyr M210 [161]. Incomplete stabilization of separated P^+ and B_A^- charges reveals itself in a smaller lowering of the $P^+B_A^-$ energy level. Calculations in the framework of molecular dynamics make it possible to estimate the characteristic time of the OH group reorientation in Tyr M210, which turns out to be close to the P^* lifetime.

An analysis of calculations by the molecular dynamics method reveals a substantial contribution of the OH group reorientation in Tyr M210 to stabilization of the $P^+B_A^-$ state. The theoretical spectrum of the autocorrelation function of fluctuations of OH-group stochastic rotations in Tyr M210 exhibit several peaks in the frequency range from 270 to 390 cm^{-1}, with the two main maxima at 356 and 368 cm^{-1} [10]. These peaks are absent in the analogous theoretical spectrum of mutant RCs lacking Tyr M210 molecules and in the resonant Raman scattering spectrum of tyrosine. Importantly, such peaks are present in the Fourier spectrum of the autocorrelation function of electrostatic energy fluctuations ΔV_{elec} in the PB and $P^+B_A^-$ states, but are absent in the analogous spectrum of fluctuations of direct P^+/B_A^- interaction electrostatic energy, ΔV_{QQ}. This once again points to the fact that 356 and 368 cm^{-1} peaks belong to the environment of P and B_A. The experimental Fourier transform spectrum of oscillations in the B_A^- absorption band at 1020 nm and in the 935–940-nm stimulated P^* emission band of native and pheophytin-modified RCs from *Rba. sphaeroides* contains weak bands in the frequency range of 300–400 cm^{-1}, resembling theoretical ones at 356 and 368 cm^{-1} [242, 243].

To summarize, results of femtosecond spectroscopy indicate the key role of the Tyr M210 mutant molecule in electron stabilization on B_A during primary charge separation in RCs. The absence of Tyr M210 in mutant RCs prevents stabilization of separated charges in the $P^+B_A^-$ state; this effect is associated with the marked slow-down of primary charge separation. The $P^+B_A^-$ state is stabilized due to the presence of the polar OH group in Tyr M210 near B_A and its reorientation under the effect of separated charges.

4.3 Role of bound water in primary charge separation

X-ray structural analysis shows that RCs of *Rba. sphaeroides* contain over 300 water molecules each, mostly on either side of the cell membrane. A small portion of these molecules are located near the P dimer and $Q_{A,B}$ quinones, as well as in the central part of the RC. Because a polar water molecule can create hydrogen bonds with the environment and donate a proton, its presence near pigments can influence charge separation in RCs.

An original hypothesis of the photoinduced reorientation of water molecules structurally connected with the P dimer during the formation of a complex with charge transfer inside the dimer was put forward in 1981 [244]. It was speculated that the P^* energy can drop by ~ 0.03 eV for 1–2 ps as the water molecule turns in the $P_A^+P_B^-$-dipole field. Fok and Borisov [244] argued that such a decrease in the P^* energy could lead to electron transfer from P^* to these water molecules and farther to bacteriopheophytin. The idea of the role of bound water molecules as possible intermediate acceptors of electrons was further developed in later research based on the known RC structure [245, 246].

As far as the mechanism of primary charge separation is concerned, there is a very interesting option between electron tunneling over the nearest atoms from P^* to B_A and electron transfer along a chain of coupled atoms (indeed, the very existence of such a chain). Of special interest in this context is the crystallographic water molecule residing in the RC structure between P_B and B_A [27, 247] (see Fig. 4). In accordance with the numeration system for the structural model of *Rba. sphaeroides* R-26 (PDB, file 1AIJ), this molecule is designated as HOH55 [248]. The B-branch of RCs contains a symmetrically located water molecule HOH30. Importantly, HOH55 is located at the distance of H-bond formation from both oxygen of the 13^1-ketocarbonyl group in B_A and nitrogen of the residue His M202 responsible for axial ligation with the Mg atom in BChl of P_B [27, 247, 248]. In other words, crystallographic data give evidence of a direct spatial connection between P_B and B_A via HOH55 and His M202.

The most straightforward method to elucidate the possible functional role of HOH55 focuses on coherent femtosecond spectroscopy of mutant RCs devoid of this water molecule but undergoing only minor structural changes compared with those in RCs of the wild type strain. The double mutant FM197R/GM203D of *Rba. sphaeroides* is one of the purple bacteria RCs studied by X-ray structural analysis that meets this criterion. One of the carboxyl oxygen molecule in the aspartic acid (Asp) residue substituting Gly M203 in its RC occupies part of the space filled with HOH55 in the wild strain RC; as a result, this water proves to be sterically displaced [249]. It is supposed that the same structural change takes place in the RCs from GM203D mutants [249]. The P^* lifetime in this mutant is known to be almost thrice as long as that in the wild strain RCs [207].

At present, opinions differ as regards causes behind the observed deceleration of primary electron transfer in RCs of mutant GM203D. Initially, the GM203D mutation was designed to add a hydrogen bond to the 13^1-ketocarbonyl group of B_A in order to lower the $P^+B_A^-$-state free energy level [207]. However, results obtained for certain RCs of *Rba. capsulatus* with a GM201D mutation (equivalent to GM203D mutation of *Rba. sphaeroides*) suggest that the $P^+B_A^-$ free energy level in this mutant is slightly higher than the P^* free energy level [165, 169]. Measurements of stimulated Raman scattering show that Asp M201 can be deprotonated and negatively charged, at least at room temperature [171]. Therefore, it was concluded that the introduction of Asp M201 decreases the midpoint redox potential (E_m) of the B_A/B_A^- coupe, which leads to a rise in the $P^+B_A^-$ free energy level and consequently to the enhancement of the P^* lifetime [171]. According to an alternative explanation, the steric displacement of HOH55 water in GM203D (GM201D) mutants prevents the hydrogen bond-mediated interaction with the 13^1-ketocarbonyl group in B_A. This interaction can stabilize B_A^- in native RCs, especially when P is oxidized during charge separation [249].

Another approach to the elucidation of the role of the HOH55 water molecule is based on the utilization of the GM203L mutant of *Rba. sphaeroides* [245, 246]. The X-ray diffraction analysis of RC crystals of this mutant reveals that replacement of Gly M203L by Leu results in the removal of HOH55 without appreciable changes in the protein structure beyond the immediate vicinity of the M203 molecule [246], because Leu M203 occupies part of the volume filled with

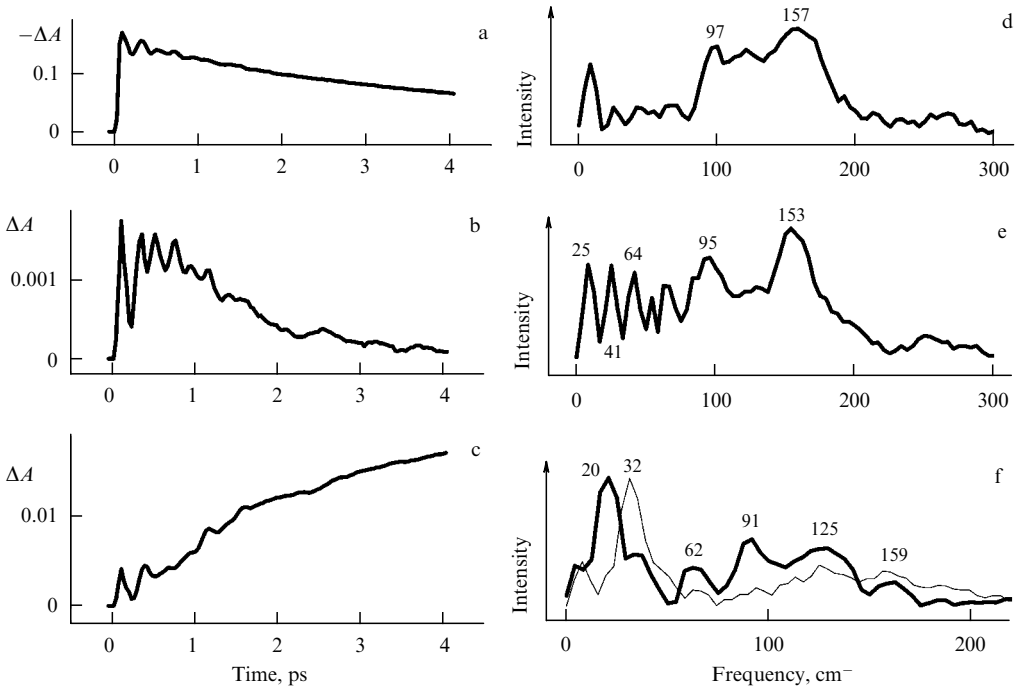

Figure 6. The ΔA kinetics (a, b, c) and Fourier transform spectra of oscillations in these kinetics (d, e, f) in the GM203L mutant RCs of *Rba. sphaeroides* for the 940-nm stimulated P^* emission band (a) and the B_A^- absorption band at 1020 nm (b), and in deuterated pheophytin-modified RCs of *Rba. sphaeroides* R-26 for the B_A^- absorption band at 1020 nm (c) [245]. The thin line in figure c is the analogous Fourier spectrum for nondeuterated RCs. Reaction centers were excited by 18–20-fs pulses with a wavelength of 870 nm at 90 K. Numerals in figures d–f stand for the frequencies of Fourier spectrum peaks.

HOH55 water in native RCs. The GM203L mutation slightly affects the His M202 conformation by rotating it a few degrees from Leu M203 about the axis roughly determined by the C–C (CG–CB) bond linking carbon-4 in the imidazole ring with beta-carbon of the side chain. This rotation has no appreciable effect on the length of the bond connecting nitrogen of NE1 in His M202 and Mg in P_B [246]. The absence of HOH55 in mutant residue GM203L is also confirmed by measurements of resonance Raman scattering, demonstrating the absence of hydrogen bond-mediated interaction with the 13^1-ketocarbonyl group of B_A in RCs of mutant GM203L, because its stretching frequency in ferricyanide-oxidized RCs (where P^+ plays the role of P) increases from 1676 to 1704 cm^{-1} [246]. Importantly, residue M203 ionization in RCs of this mutant does not influence the initial electron transfer reaction, which could complicate the analysis of results.

The study of the ΔA kinetics in RCs of mutant GM203L revealed that the decline of stimulated P^* emission at 90 K in its long-wavelength maximum at 940 nm occurs with the principal time constant of ~ 4.3 ps (Fig. 6), which is almost 4 times as large as in native RCs [245]. In other words, the GM203L mutation significantly increases the P^* lifetime. The fall in P^* emission is accompanied by very apparent oscillations. Their Fourier spectrum in mutant RCs differs from that in native RCs in the presence of a suppressed 125-cm^{-1} mode.

The mutant GM203L exhibits a B_A^- absorption band at 1020 nm that appears with a 113-fs delay after P excitation in response to electron transfer from the excited P^* state to B_A (Figs 6, 7). This electron transfer is a reversible process, and the B_A^- absorption in the case of a 206-fs delay significantly decreases. The next increase in the absorption band at 1020 nm occurs 331 fs after P excitation. The 1020-nm band in GM203L mutant RCs exists no longer than 2–3 ps, as in native RCs.

Phases of rise and fall can be distinguished in the ΔA kinetics of the B_A^- absorption band at 1020 nm in both mutant and native RCs against the background of strong oscillations. This fact confirms the two-step mechanism of electron transfer in GM203L mutant RCs following the $P^* \rightarrow B_A \rightarrow H_A$ scheme. In mutant RCs, these phases are slower than in native RCs. The main difference between the

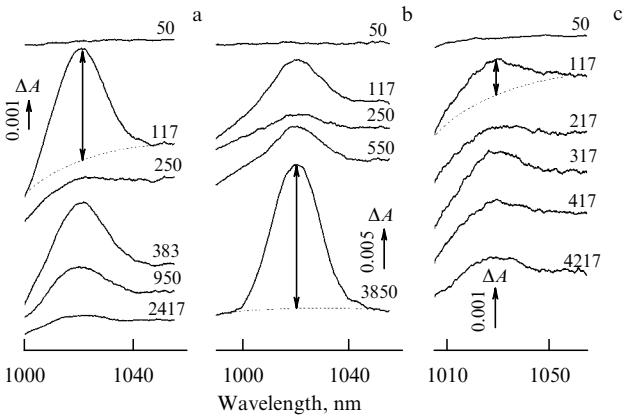

Figure 7. Differential (light–dark) absorption spectra at certain femtosecond delays relative to the onset of excitation for native (a) and pheophytin-modified (b) RCs from *Rba. sphaeroides* R-26 and RCs of *Cfx. aurantiacus* (c) excited at 90 K by 25-fs pulses with a wavelength of 870 nm [242, 243]. Double-headed arrows indicate amplitudes of the bands used to construct kinetics. Numerals above the curves mark delays in femtoseconds after the onset of excitation. The curves are displaced vertically for clarity.

Fourier spectra of oscillations in a B_A^- absorption band in mutant (see Figs 6, 7) and native RCs lies in the absence of 32- and 127-cm^{-1} modes in the former. These modes predominate in the Fourier spectra of native RCs for the B_A^- band. Other modes of the Fourier spectrum of oscillations in the 1020-nm band of mutant RCs with frequencies of 25, 41, 64, 95, and 153 cm^{-1} practically coincide with those of oscillations of stimulated P^* emission within an accuracy of 2–4 cm^{-1}. The ΔA kinetics at 760 nm for mutant (GM203L) and native RCs, reflecting electron transfer from B_A^- to H_A are qualitatively similar. The characteristic time of the $P^+H_A^-$ state accumulation in mutant RCs is several times as large as in native RCs. Bleaching of the H_A band in mutant RCs is accompanied by weak oscillations, as in native RCs. The Fourier spectrum of oscillations at 760 nm in mutant RCs does not contain the 32-cm^{-1} band typical of analogous spectra of native RCs. Similar changes are observed in the kinetics of the aforementioned bands for dry films of RCs from *Rba. sphaeroides* R-26.

Let us turn to results obtained for deuterated RCs from *Rba. sphaeroides* R-26 at 90 K [245]. Both native and pheophytin-modified RCs were deuterated. Substitution of the HOH buffer by a DOD buffer caused no destructive changes to the RC structure, as follows from the unaltered shape and spectral position of the B_A^- absorption band at 1020 nm and the H_A absorption band at 760 nm, as well as from invariability of the typical decay time constants of stimulated P^* emission, band H_A bleaching, and band B_A^- dynamics.

Primary charge separation in deuterated RCs is accompanied by oscillations in all these spectral bands. The amplitudes and characteristic decay times of these oscillations are similar to those for RCs in an HOH buffer. The main outcome of RC deuteration consists in altering the Fourier spectra of these oscillations. Deuterated RCs, i.e., RCs in the DOD buffer, undergo a general decrease in the frequencies of all characteristic bands in Fourier spectra of oscillations in the 50–200-cm^{-1} range in contrast to the respective frequencies for RCs in the HOH buffer, which corresponds to a longer oscillation period (Fig. 6c, f for the B_A^- absorption band). This shift has a coefficient of ≈ 1.4–1.6 in both native and pheophytin-modified RCs. Because the intense narrow 32-cm^{-1} band predominates in the Fourier spectra of B_A^- and H_A absorption oscillations in nondeuterated RCs, its low-frequency shift upon RC deuteration is especially apparent. The shift of other bands in the Fourier spectra of stimulated P^* emission oscillations, as well as in B_A^- and H_A absorption oscillations, can be masked by changes in their relative amplitudes. The shift of the center of the broad 130-cm^{-1} band in the Fourier spectra of P^* and B_A^- oscillations upon RC deuteration has the same coefficient as the shift of the 32-cm^{-1} band.

Thus, the removal of water from RCs or its replacement by heavy water affects first and foremost the 32-cm^{-1} mode of oscillations in the B_A^- absorption band at 1020 nm and some higher-frequency modes in oscillations of stimulated P^* emission at 940 nm and B_A^- absorption at 1020 m. In native RCs, these modes have frequencies very close to those divisible by 32 cm^{-1}, which points to their belonging to overtones of the 32-cm^{-1} fundamental mode. With the water removed, the 32-cm^{-1} mode and multiple modes disappear from the GM230L mutant RCs, while RC deuteration displaces all these modes downward along a frequency scale with roughly the same coefficient. Because HOH55 water is admittedly absent in GM230L mutant, the disappearance of the 32-cm^{-1} mode and multiple modes from the RC kinetics of this mutant implies that this mode is inherent in the HOH55 water molecule.

The appearance of higher harmonics (up to the seventh one) in oscillations is more characteristic of rotational than vibrational modes. The water molecule in the gaseous phase is known to undergo rotation of three types with characteristic frequencies of 20, 32, and 52 cm^{-1} [250]. The rotational frequency of 32 cm^{-1} exactly corresponds to the frequency of the experimentally detected oscillation mode, while the difference between two other frequencies equals 32 cm^{-1} as well.

It is quite simple to estimate the isotopic shift for the intense narrow 32-cm^{-1} mode farthest from the 130-cm^{-1} vibrational band. An experimentally found value of this shift is ≈ 1.6, or higher than theoretical one (1.375) for the shift of vibrational bands of proton-containing molecular groups, but lower than the calculated value (1.8) for the shift of rotational bands of these groups. This discrepancy arises from incomplete deuteration or its absence in certain parts of RCs. The presence of glycerol containing OH groups in the RC buffer during low-temperature measurements increases the probability of obtaining DOH molecules (isotopic ratio 1.422) instead of DOD. The totality of available data indicates that the 32-cm^{-1} mode in oscillations of $P^+B_A^-$ and $P^+H_A^-$ products corresponds to one of the rotational frequencies of water molecules.

The very apparent deceleration of P^* emission damping in GN203L mutant RCs is a very remarkable consequence of HOH55 removal from these RCs. A comparison of results of X-ray analysis of the structure of GN203L mutant and native RCs excludes an appreciable alteration of their conformation caused by this mutation. The midpoint redox potential E_m of the P/P^+ couple in GM203L mutant RCs is the same as in native ones [246]. It can be expected that the absence of an H-bond between the ketocarbonyl group of B_A and HOH55 water in the GM203L mutant will change the value of E_m for the B_A/B_A^- couple, but there are thus far no data confirming this conjecture. Nor are there reports allowing us to conclude whether a hydrogen bond between B_A and HOH55 forms during the lifetime of the $P^+B_A^-$ state. This does not permit excluding the probability that GM203L mutation changes the energy characteristics of the primary charge separation reaction.

The P^* lifetime in GM203L mutant RCs (4.3 ps) coincides with that of a minor component (having an amplitude 15–20% that of the major component) of stimulated P^* emission kinetics in native RCs. The disappearance of the basic component of electron transfer with a lifetime of 1.2 ps (responsible for 80–85% of the electron transport in native RCs) after the removal of HOH55 water molecules from the RC structure suggests the disappearance of the most probable electron transfer pathway. The slower component (4.3 ps) may reflect the existence of other (less efficient) pathways of electron traffic from P^* to B_A. The position of the HOH55 water molecule is such that it is localized within the next chain of polar atoms: $N-Mg(P_B)-N-C-N(His\,M202)-HOH55-O=(B_A)$, which connects P donor and B_A acceptor and can be involved in electron transfer (see Fig. 4). In this context, the enhanced P^* lifetime in the GM203L mutant appears to reflect disintegration of this chain due to HOH55 water elimination.

Results of quantum-mechanical calculations indicate that the maximum density of π-electrons in the P^* state is localized

on nitrogen atoms linked to the central Mg atom in a P_B molecule [241], meaning that the nitrogen atom ligating the Mg atom in His M202 mutant residue is also very close (within 2 Å) to the maximum spin density region in P_B. The aforementioned chain of polar groups maintains the principal (80–85%) high-rate ($1/1.2\ ps^{-1}$) electron transfer pathway in native RCs. Its disruption in the absence of HOH55 water molecules significantly reduces the electron transport rate ($1/4.3\ ps^{-1}$) and makes electron transfer proceed along other ('nonspecific') tunneling routes. This slow traffic accounts for no more than 5–20% of the total in native RCs but prevails in GM203L mutant reaction centers. It is worthwhile to note that the above-mentioned bridge formed by polar groups is longer than the shortest electron tunneling route across the space between P_A/P_B and B_A (roughly 8.5 Å compared with 3.5–5.5 Å). The higher rate of electron transfer along this bridge is due to the fact that the chain of polar groups creates a more efficient medium for electron tunneling than a vacuum and thereby makes up for the difference in distance. Specifically, the H-bond forms an electron tunneling medium almost thrice as efficient as a vacuum [251].

Analysis of the data reported in Ref. [245] allows us to conclude that rotation of HOH55 water following femtosecond excitation of RCs influences, regardless of the cause behind the slow-down of P^* decay in GM203L mutant RCs, the dynamics of electron transfer from P^* to B_A. A hydrogen bond between HOH55 water and B_A as strong as ≈ 4 kcal mol^{-1} is readily identified in oxidized RCs of *Rba. sphaeroides* by Raman spectroscopy, but is not recorded in neutral RCs [246]. This means that this bond forms during charge separation in response to the appearance of the positive charge on P^+ and the negative charge on B_A^- that rotate the water dipole. The water molecule stops rotating after 1–3 revolutions at a frequency of 32 cm^{-1}. Formation of the H-bond between HOH55 and B_A promotes $P^+B_A^-$ state stabilization. Water molecule rotation causes periodic electron transfer from P_B to B_A and back with a frequency of 32 cm^{-1}. The periodic appearance of additional electron density on B_A^- at an early stage of charge separation, when populations of the P^* and $P^+B_A^-$ states are roughly identical, can just as well promote stabilization of the B_A^- state. Such stabilization occurs faster than the relatively slow relaxation of the surrounding molecules toward a new electron configuration.

It can be concluded that an HOH55 molecule of crystallographic water in the RC of *Rba. sphaeroides* plays an important role in electron transfer from the primary electron donor P^* to the primary acceptor B_A. The X-ray structural analysis of RCs demonstrates that HOH55 water can be involved in one of the pathways for the efficient electron transfer along the chain of polar atomic groups connecting the P dimer and the B_A monomer. Femtosecond excitation of RCs induces HOH55 molecule rotation and thereby modulates populations of primary $P^+B_A^-$ and $P^+H_A^-$ states with separated charges.

5. Participation of monomeric bacteriochlorophyll B_A in primary charge separation

5.1 Position of the $P^+B_A^-$ energy level

Of primary importance for evaluating the participation of B_A in direct electron transfer is the position of the $P^+B_A^-$ state free energy level with respect to that of the excited P^* state. Given that the $P^+B_A^-$ level lies below the P^* level, the usual electron transfer from P^* to B_A can occur. If, however, the $P^+B_A^-$ level is above the P^* level, only virtual participation of the B_A vacant electron energy level in electron transfer from P^* to H_A is possible by the quantum superexchange mechanism [252]. There are a few ways to determine the $P^+B_A^-$ energy level.

One is to calculate $BChl^-$ and $BPhe^-$ solvation energies in a solution and the analogous $P^+B_A^-$ and $P^+H_A^-$ energies in RCs taking account of the measured values of the midpoint redox potential for BChl and BPheo in the respective solutions [93, 159, 253–255]. The calculated solvation energy includes the donor–acceptor electrostatic interaction and the influence of the environment. The $P^+B_A^-$ energy in the gaseous phase can also be calculated by the quantum-mechanical methods [94, 173, 256–262]. The calculations take into consideration dielectric shielding in the framework of the Poisson–Boltzmann equation with macroscopic dielectric constants [94, 263] or in the framework of the Langevin microscopic dipole model [94, 254, 264]. Either the spherically symmetric [159, 264–267] or periodic [268, 269] dipole location model is applied in the calculations. Molecular dynamics methods in combination with the computational methods of free energy perturbations make it possible to estimate the influence of changes in the protein environment on the $P^+B_A^-$ energy [159, 160, 253–255]. Calculations of molecular dynamics with the involvement of data on the RC crystal structure in *Rba. sphaeroides* [27] give the difference between P^* and $P^+B_A^-$ free energies as on the order of -2 kcal mol^{-1}, and the reorganization energy of reaction $P^* \rightarrow P^+B_A^-$ as ~ 2 kcal mol^{-1} [159, 160]. A similar result was obtained in calculations for RCs from *Blc. viridis* [93, 218, 254, 270, 271]. The low accuracy (± 2 kcal mol^{-1}) of these calculations does not rule out the $P^+B_A^-$ energy level lying somewhat higher than the P^* level. In fact, some theoretical studies predict that the $P^+B_A^-$ level is significantly higher than the P^* level [94, 258, 259, 261]. A thorough analysis of these data revealed a number of inaccuracies associated with taking account of dielectric shielding effects [218, 254, 269].

Evaluation of the $P^+B_A^-$ free energy level based on experimental results of femtosecond spectroscopy of the pheophytin-modified RCs gives the value of ~ -0.06 eV (or 1.4 kcal mol^{-1}) relative to the P^* level [272, 273]. Comparing electron transfer rates in mutant and native RCs makes it possible (provided mutation-induced changes in the $P^+B_A^-$ level are known from the theory or experiment) to find the absolute value of the $P^+B_A^-$ energy from a theoretical expression for the transfer rate in which this energy is included as a parameter [43, 44, 65–67, 207, 208, 223, 274–281]. Expression for the transfer rate can be derived based on classical or quantum-mechanical representations. The results of such comparisons indicate that the $P^+B_A^-$ energy level is close to or somewhat lower than the P^* level.

One more approach to determining the difference between the P^* and $P^+B_A^-$ energies consists in measuring slowed down fluorescence associated with $P^+B_A^-$ recombination giving rise to P^*. Pheophytin-modified RCs of *Rba. sphaeroides* R-26 are the most suitable for the purpose, since the replacement of their H_A by plant pheophytin $\Phi\phi_A$ prolongs the lifetime of the $P^+B_A^-$ state [282]. It was found that the temperature dependence of the fluorescence of pheophytin-modified RCs with prereduced quinones becomes increasingly and reversibly stronger as temperature rises within a range from 95 to 200 K [282]. A less pronounced fluorescence rise with

temperature occurs in pheophytin-modified RCs in the absence of a reducing agent. In native RCs, the temperature dependence of fluorescence remains unaltered as temperature increases. Temperature dependences of fluorescence yield were obtained in the framework of the charge separation model for native and pheophytin-modified RCs taking into consideration reverse transitions, recombination, and 'rapid' fluorescence. An approximation of experimental temperature dependences using theoretical approaches leads to the conclusion that the $P^+B_A^-$ energy level in pheophytin-modified RCs of *Rba. sphaeroides* R-26 is ~ 550 cm^{-1} below the P^* level [282]. Because such a modification does not affect B_A and P molecules, there is every reason to believe that this inference holds for native RCs of *Rba. sphaeroides* R-26, too.

The difference between P^* and $P^+H_A^-$ free energies can be derived from measurements of the equilibrium constant for these states in RCs with preliminarily reduced Q_A or RCs without Q_A. Under these conditions, P^* fluorescence quenching occurs with the principal time constant of 10–20 ns, coincident with the damping constant of the $P^+H_A^-$ state [42, 283–293]. Minor (faster) components of P^* fluorescence can be related to $P^+H_A^-$ relaxation. It was found from the relative amplitude of the major (slow) component of P^* fluorescence that the free energy level of the relaxed $P^+H_A^-$ state is present much lower (by 0.21–0.26 eV) than that of the P^* state.

Another method for determining the free energy of $P^+H_A^-$ consists in finding the equilibrium constant of the $P^+H_A^-$ state and the excited triplet state (^{3}P) of P. The ^{3}P state in RCs of *Rba. sphaeroides* with the inhibited $H_A^- \rightarrow Q_A$ reaction arises from $P^+H_A^-$ with a quantum yield of $\sim 30\%$ at 295 K [294]. It was shown by measuring fluorescence spectra [295] and determining the activation energy for the thermal population of the excited singlet state [108] that the ^{3}P level lies 0.42 eV below the P^* level. Degradation of the ^{3}P state is mostly due to reverse transition to the $P^+H_A^-$ state under the influence of heat and subsequent recombination into the ground state. An external magnetic field affects both the formation and decay of the ^{3}P state, since these processes involve the singlet and triplet forms of $P^+H_A^-$ in which the difference between energy levels is proportional to the magnetic field strength [296–299]. Studies of the influence of the magnetic field and temperature on $P^+H_A^-$ decay kinetics showed that the $P^+H_A^-$ level is located 0.25–0.26 eV lower than the P^* level [291, 295, 300–302].

Summing up experimental and theoretical findings, it can be concluded that the $P^+B_A^-$ energy level is $\sim 0.04-0.07$ eV lower than the P^* level [54, 65, 165, 167, 168, 272, 273, 275, 276, 282] and $\sim 0.2-0.3$ eV higher than the $P^+H_A^-$ level, which means that the B_A molecule can really participate in electron transfer from P^* to H_A.

5.2 Participation of a B_A molecule in primary charge separation

The long-standing problem of the involvement of monomeric bacteriochlorophyll (B_A) molecules in primary charge separation in the capacity of intermediate acceptors (see reviews [2, 7]) arises logically from the location of B_A between P and H_A molecules, as shown by X-ray structural analysis (see Fig. 1) [22, 27]. Conclusive evidence of the direct participation of B_A in charge separation processes has remained elusive for a long time.

The first experimental data suggesting the possibility of an electron's appearance on B_A were obtained by picosecond measurements in RCs of *R. rubrum* [303], and thereafter in RCs of *Rba. sphaeroides* [304]. The authors observed P band bleaching and partial bleaching of the B band that occurred with a roughly 1.5-ps delay after the onset of excitation; they interpreted these observations as reflecting the formation of the mixed $P^+B_A^-/P^*$ state.

One of the first femtosecond measurements within the 700–900 nm range in modified RCs of *Rba. sphaeroides* lacking B_M molecules was reported in Refs [305, 306]. The thorough analysis of ΔA kinetics and spectra in these studies confirmed the formation of the $P^+B_A^-$ state having approximately the same population as the $P^+H_A^-$ state by virtue of a rapid exchange of an electron between B and H. Nevertheless, measurements and analysis of the ΔA kinetics in this spectral range with a femtosecond resolution by many other authors failed to demonstrate the formation of the $P^+B_A^-$ state [33, 35, 36].

The results of pico- and femtosecond spectroscopy gradually brought researchers to a better understanding of the main difficulty hampering detection of the $P^+B_A^-$ state that arises from the fact that $P^+B_A^-$ formation takes several fold more time than its degradation due to electron transfer from B_A^- to H_A [39, 307]. This accounts for the poor population of the $P^+B_A^-$ state during the entire period of its existence (a few picoseconds). Another difficulty is that the $P^+B_A^-$ state spectrum is strongly masked by the spectra of other states in the visible range, where the overwhelming majority of measurements are made. Femtosecond excitation of P resulting in stimulated P^* emission gave rise to a fast component possibly related to the two-step electron transfer from P^* to H_A [39–41, 163]. However, this effect could not be distinguished against the background of oscillations associated with the motion of the nuclear wave packet and temporal shifts of the P^* emission band.

Difficulties encountered in the first attempts to observe the $P^+B_A^-$ state gave rise to an idea of virtual (as opposed to real) participation of B_A in electron transfer by the superexchange mechanism [252, 308] responsible for quantum-mechanical mixing of the $P^+B_A^-$ state with both P^* and $P^+H_A^-$ states. Analysis of kinetic measurements in the 1020-nm range revealed (within the limits of measurement error) a weak absorption band that could be associated with the B_A^- anion [307, 309]. It was identified for the first time in a $BChl^-$ anion solution in Ref. [96]. In RCs of *Rba. sphaeroides*, electron transfer at room temperature from P^* to B_A and from B_A^- to H_A can proceed with rate constants of ~ 3.5 ps and ~ 0.9 ps, respectively [307]. If the two reactions are assumed to be reversible, the rate constant of $\sim 1-3$ ps holds for either of them [43, 309].

The most convincing evidence of real participation of B_A in two-step electron transfer from P^* to H_A was obtained for RCs of *Rba. sphaeroides* in which bacteriopheophytin H_A was replaced by plant pheophytin (Pheo-a) [107, 272, 273, 310] or bacteriochlorophyll [167, 168]. As the redox potentials of Pheo and BChl are shifted toward negative values with respect to the BPhe redox potential, these substitutions increased the amplitude and the time of absorption changes associated with the $P^+B_A^-$ state formation. In other words, these modified RCs accumulate the $P^+B_A^-$ state in the picosecond range.

The first direct registration of the B_A^- absorption band at 1020 nm in Pheo-modified RCs at 5 K was reported in Ref. [107]. The replacement of amino acid residue Phe near H_A by aspartic acid increasing the free energy of $P^+H_A^-$ in the case of Asp ionization, caused a similar deceleration of the $B_A^- \rightarrow H_A$ reaction [166, 280]. Mutations heightening the

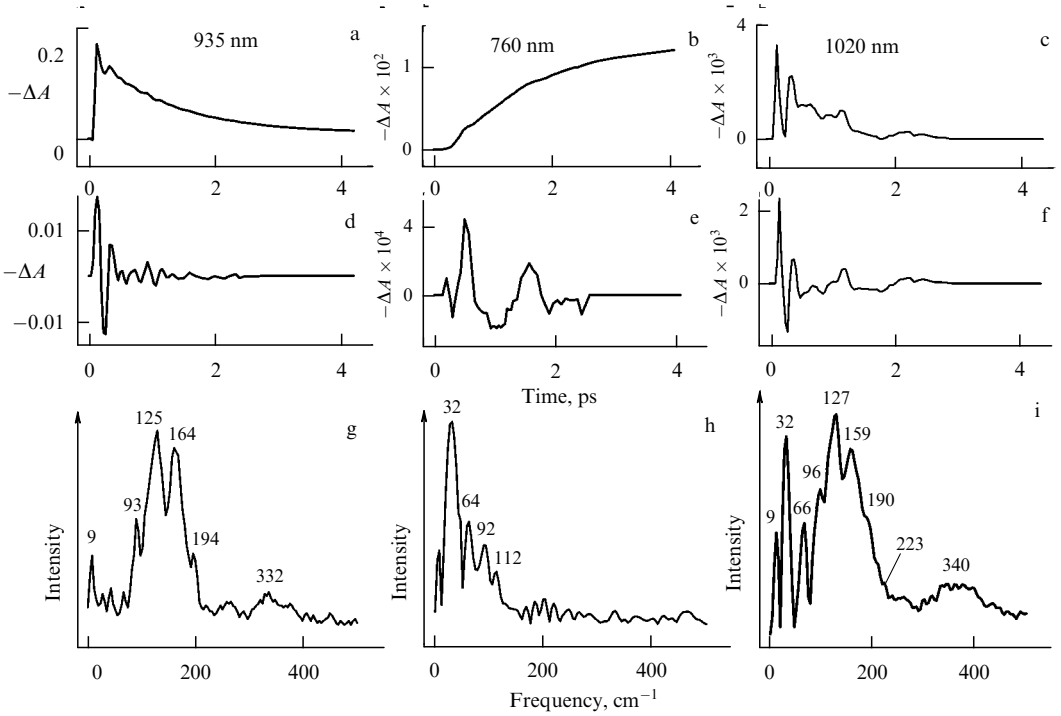

Figure 8. The ΔA kinetics (a–c), their oscillating component (d–f), and the Fourier transform spectrum of the oscillatory component (g–i) for the absorption band of B_A^- at 1020 nm, 935-nm stimulated P^* emission bands, and absorption band of H_A at 760 nm in native RCs of *Rba. sphaeroides* R-26 excited at 90 K by 25-fs pulses with a wavelength of 870 nm [242, 243]. Numerals in figures g–i stand for the frequencies of the Fourier spectrum peaks.

$P^+B_A^-$ energy level also slowed down primary charge separation by retarding the rate of the $P^* \rightarrow B_A^-$ reaction [64–67, 75, 114, 163, 164, 280]. The substitution of BChl B_A by bacteriopheophytin H (BPhe) in mutants gave rise to the formation of a long-lived P^+BPhe^- state corresponding to a lowering in its free energy in comparison with the free energy of the initial $P^+B_A^-$ state [224].

The real participation of the B_A molecule in electron transfer in native RCs was considered in Refs [242, 243, 311], where ΔA spectra were measured in wavelength ranges from 909 to 1070 nm (stimulated P^* emission band and B_A^- anion absorption band) and from 730 to 790 nm (H_A absorption band) in RCs of *Rba. sphaeroides* R-26 and *Cfx. aurantiacus* at 90 K (see Fig. 7). Control measurements were made for pheophytin-modified RCs of *Rba. sphaeroides* R-26 in which the $P^+B_A^-$ state is known to accumulate in the picosecond time range. They revealed a weak B_A^- absorption band with the center at 1020 nm in RCs of *Rba. sphaeroides* R-26 and at 1028 nm in RCs of *Cfx. aurantiacus*. The shape of this band was identical to the B_A^- absorption band in peophitin-modified RCs of *Rba. sphaeroides* R-26.

The shape and spectral position of the revealed band remain unaltered in the picosecond range, but its amplitude changes with time in a complicated oscillatory manner (see Fig. 7). The first most intense maximum in oscillations of the B_A^- band amplitude occurs with a lag of 120 fs; it is followed by several less intense peaks. The B_A^- absorption band totally disappears in the case of a $\geqslant$ 2.5-ps delay, which suggests further electron transfer from B_A^- to H_A.

The mathematical discrimination of oscillations in the nonoscillatory part of ΔA kinetics at 1020 nm reveals the phase of rise with a time constant of $\sim$ 0.2 ps, followed by the phase of fall with a time constant of $\sim$ 0.8 ps. The monotonic rise of the B_A^- absorption band in pheophytin-modified RCs reflects accumulation of the $P^+B_A^-$ state, which is accompanied by damping oscillations. It facilitates studying oscillations for $>$ 1-ps delays. The fall in stimulated P^* emission at 935 nm in native and pheophytin-modified RCs has the principal time constant of $\sim$ 1.2 ps at 90 K, and is also accompanied by rapidly damping oscillations (Fig. 8). These oscillations are in phase with oscillations in the B_A^- absorption band. Bleaching of the H_A absorption band at 760 nm in native RCs of *Rba. sphaeroides* R-26 reflects the appearance of an electron on H_A with a time constant of $\sim$ 1.2 ps at 90 K (Fig. 8). The ΔA kinetics at 760 nm have a small time lag of $\sim$ 0.2 ps at 90 K, suggesting the delayed appearance of an electron on H_A due to its earlier appearance on B_A. Bleaching of the H_A absorption band at 760 nm is accompanied by weak oscillations roughly corresponding to the integration of B_A^- band oscillations over time, which suggests the efficient electron transfer from B_A^- to H_A.

Fourier transform spectra of oscillations at 935, 1020, and 760 nm contain several bands and have an intricate shape (see Fig. 8). The Fourier spectrum of stimulated P^* emission oscillations at 935 nm is dominated by a broad band with the center at 130 cm^{-1}, in which a few narrower bands separated by 25–35-cm^{-1}, intervals can be distinguished. This spectrum largely reflects vibrational motions inside the P dimer with a fundamental period of around 250 fs [131–134]. The Fourier spectrum of B_A^- band oscillations at 1020 nm has a wide 130-cm^{-1} band along with lower-frequency bands, among which the intense 32-cm^{-1} band corresponding to the oscillation period of $\sim$ 1 ps is especially apparent. The 32-cm^{-1} mode particularly stands out in B_A^- band oscillations in pheophytin-modified RCs, where it predominates. The Fourier spectrum of H_A band oscillations at 760 nm mostly consists of narrow bands in the 10–120-cm^{-1} frequency range, which is dominated by the 32-cm^{-1} band.

Thus, the 130-cm^{-1} mode of nuclear movements is conjugated to the $P^* \rightarrow P^+B_A^-$ reaction, and the 32-cm^{-1} mode to the $P^+B_A^- \rightarrow P^+H_A^-$ reaction.

The dynamics of the stimulated P^* emission band at 940 nm, and the B_A^- and H_A absorption bands at 1028 and 750 nm, respectively, in RCs of *Cfx. aurantiacus* are qualitatively similar to those in RCs from *Rba. sphaeroides* R-26. The phase of rise of the nonoscillating component of ΔA kinetics at 1028 nm has a time constant of ~ 1 ps at 90 K, while the time constant of the phase of fall is about 5 ps. The time of P^* quenching and H_A bleaching in RCs of *Cfx. aurantiacus* at 90 K is ≈ 5 ps, which suggests a slower charge separation than that in RCs of *Rba. sphaeroides*. The B_A^- absorption band at 1028 nm undergoes weak oscillations, with the frequency spectrum containing a broad band at approximately 150 cm^{-1} and several narrower bands at 35, 52, and 72 cm^{-1}. Oscillations in the H_A absorption band occur within a similar frequency range, whereas oscillations of the stimulated P^* emission band are dominated by frequencies of ≈ 150 cm^{-1}.

To sum up, the data reported in Refs [242, 243, 311] indicate that primary charge separation in RCs of *Cfx. aurantiacus* and *Rba. sphaeroides* constitutes a two-step process: $P^* \rightarrow P^+B_A^- \rightarrow P^+H_A^-$ [287], in which B_A directly participates. This classical irreversible process of electron transfer is accompanied by reversible oscillatory transfer associated with the motion of the nuclear wave packet.

5.3 Motion of a wave packet in charge separation

The available data allow the movements of the nuclear wave packet over the potential energy surfaces of various states to be described in more concrete terms (Fig. 9). In native RCs of *Rba. sphaeroides* R-26, the $P^+B_A^-$ energy level lies ~ 550 cm^{-1} below the P^* level, while the $P^+H_A^-$ level is ~ 1500–2000 cm^{-1} below P^*. The $P^+B_A^-$ potential surface intersects the P^* surface at its right long-wavelength slope not far from the bottom, so that the activation energy of the $P^* \rightarrow P^+B_A^-$ reaction does not exceed a few dozen cm^{-1}. Similarly, the $P^+H_A^-$ surface intersects the $P^+B_A^-$ surface near its bottom. The surfaces split into upper and lower ones at the intersection points. The energy gap between the split P^* and $P^+B_A^-$ surfaces ranges $\sim 10-30$ cm^{-1} [177].

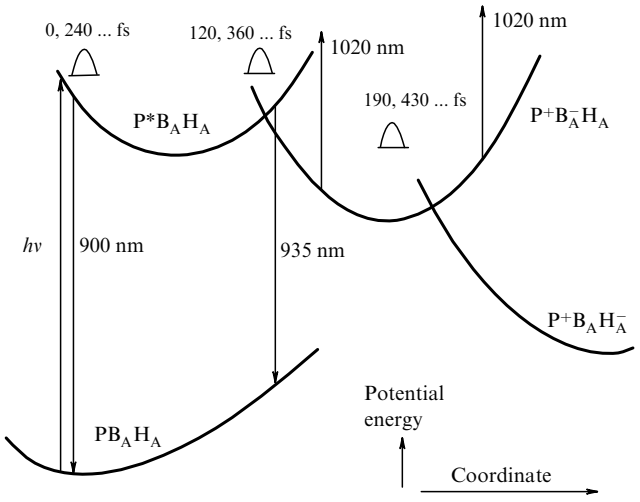

Figure 9. Simplified single-coordinate diagram of nuclear wave packet movements over the potential energy surface of the PB_AH_A ground state, excited $P^*B_AH_A$ state, and the $P^+B_A^-H_A$ and $P^+B_AH_A^-$ states with separated charges (abbreviated notations P, P^*, $P^+B_A^-$, and $P^+H_A^-$ are also used in the text).

The wave packet formed by a few vibrational sublevels arises at the left short-wavelength slope of the P^* surface, where it exhibits emission at ~ 900 nm. Then, the packet starts to move over the P^* surface toward the long-wavelength slope and reaches the intersection point of P^* and $P^+B_A^-$ surfaces within ~ 120 fs. At this instant, there is emission from the wave packet at 935 nm. At the intersection point, the part of the wave packet gives way to the $P^+B_A^-$ surface, retaining coherent motion; this results in appearing the B_A^- absorption band. This part of the packet travels over the $P^+B_A^-$ surface and with a lag of ~ 190 fs it reaches the region where it intersects the $P^+H_A^-$ surface onto which it passes in part and thereby increases bleaching of the H_A band. The main part of the packet remains on the P^* surface and begins to move backward after it reaches its edge. The turning point lies near the P^*–$P^+B_A^-$ intersection point. In so doing, the wave packet again finds itself near the intersection point after a time delay of ~ 360 fs, and the process repeats itself.

Circulation of the wave packet is accompanied by its decay and smearing due to dissipation and relaxation. The real motion of the wave packet over each of the surfaces has an intricate character; it occurs simultaneously in different directions at several frequencies, among which at least two fundamental modes (130 and 32 cm^{-1}) can be distinguished. The relative contribution of different modes to the overall picture of vibrations in the product depends on their projections onto the direction of the primary $P^* \rightarrow P^+B_A^-$ reaction. The complicated character of the wave packet motion may be due to surface anharmonicity or reflect the formation of multimode hypersurfaces. The invariable shape of the B_A^- absorption band in time suggests the absence of $P^+B_A^-$ and $P^+(B_A^-)^*$ surfaces shifting along the coordinate. In this case, the motion of the wave packet over the $P^+B_A^-$ surface cannot be visualized, but its presence on this surface is confirmed by oscillations in the H_A^- absorption band. The character of oscillations in the B_A^- absorption band point to an essential reversibility of electron transfer due to the packet motion at 130 cm^{-1}.

In principle, the transport coefficient of a wave packet motion from one surface to another depends on the time of its stay in the vicinity of the transfer region and the energy spectrum width. The less time the packet remains near the transfer region and the wider its energy spectrum compared with the energy gap width at the surface splitting point, the smaller the part of the packet that gives may to the other surface. The characteristic time during which the 130-cm^{-1} mode remains near the surface intersection site is ~ 100 fs; it increases to ~ 600 fs for the 32-cm^{-1} mode, which accounts for enhanced electron transfer irreversibility at this frequency. The rate of packet's oscillatory motion being proportional to the oscillation frequency, the probability of transfer for high-frequency modes is smaller than for low-frequency ones, meaning that the low-frequency fraction in product oscillations is larger than in donor oscillations, as completely confirmed by experiment. The filtration of low-frequency oscillations is especially apparent in the absorption band of the secondary product H_A^-.

The Redfield theory [312] can be applied to simulate electron transfer dynamics for the case of strong coupling between the P^* and $P^+B_A^-$ electronic states and two vibrational modes at 130 and 32 cm^{-1} [313]. Such a model takes into account four electronic states, viz. the ground state of the

primary donor P, its excited state P^*, the primary state with separated $P^+B_A^-$ charges, and the excited state $P^+(B_A^-)^*$. The potential energy surfaces of P^* and $P^+B_A^-$ states depend on two efficient nuclear coordinates. The first reaction coordinate is related to the shift of the P^* state with respect to P, which results in the formation of a nonequilibrium vibrational state in the case of P excitation and in coherent oscillations of the wave packet at 130 cm^{-1}. The shift of the $P^+B_A^-$ surface along the second reaction coordinate causes oscillatory motion along this coordinate with a frequency of 32 cm^{-1}. Such additional motion gives rise to 32-cm^{-1} oscillations in the $P^+B_A^-$ state superimposed on 130-cm^{-1} oscillations penetrating into this state from the P^* state.

Due to the electronic conjugation of P^* and $P^+B_A^-$ states, the 32-cm^{-1} mode penetrates onto the P^* surface and generates oscillations at this frequency in stimulated P^* emission kinetics. Simulations show that the moderate potential barrier between the P^* and $P^+B_A^-$ states along the reaction coordinate corresponding to the 130-cm^{-1} mode accounts for the high packet penetration rate into the product region [313]. The shift of the packet along the second coordinate corresponding to the 32-cm^{-1} mode leads to irreversible charge separation. Calculations in Ref. [313] show that a combination of two collective nuclear modes increases the forward reaction rate and decreases the rate of the reverse reaction.

In the cases of coherent and incoherent excitations, the efficiencies of electron transfer determined by the configuration of the donor and product's potential surfaces are practically identical. In experiment, coherent oscillations only modulate the transfer dynamics but its total rate remains the same as in natural photosynthesis (where wave packets are absent). However, coherent (and long-lived) oscillations help to visualize contributions from various collective nuclear modes at different stages of the reaction and, as a result, make it possible to determine the main reaction coordinates and configuration of the respective potential surfaces. Relatively longer oscillation lifetimes are due to coherence transfer in the course of vibronic relaxation, including the transfer of coherence from one mode to another. Thus, coherent oscillations along the first reaction coordinate, induced by pulse-mediated excitation in the primary donor region, stand up during the motion along the second coordinate as well. Mathematically, this is related to nonsecular terms of the Redfield relaxation tensor [312], also responsible for the relationship between coherences and populations of the vibronic levels.

It should be noted that population oscillations of different RC states can reflect coordinated movements of pigments and their environment. Recent *ab initio* calculations of molecular dynamics have shown that some vibrational modes of the P nearest environment with frequencies in the 30–100-cm^{-1} range influence primary charge separation in RCs of *Rba. sphaeroides* [314, 315]. According to these calculations, the 100-cm^{-1} mode reflects the collective vibrational motion of P and His M202 rotation. This mode participates in charge separation inside the P dimer and manifests itself in the P^* dynamics. The 30–35-cm^{-1} mode reflects the collective motion of the water molecule and the neighboring molecules (having H-bonds with the water molecule) near the P dimer.

The study of P dimer molecular dynamics [316] has shown that vibrational motions of His 172, His 202, and protein α-helices with frequencies from 30 to 120 cm^{-1} influence the formation of the $P_A^+P_B^-$ dipole in *Rba. sphaeroides* RCs. Certain low frequencies of oscillations of the nearest environment of P are very close to oscillations frequencies in RC kinetics [130–135] and resonance Raman scattering frequencies for the P dimer [317, 318]. This fact appears to reflect the collective character of these oscillations for correlated coherent and incoherent movements inside and outside the P dimer.

To summarize, the B_A molecule is the primary electron acceptor in RCs. Studies of the femtosecond dynamics for the B_A^- absorption band at 1020 nm fully support the validity of the scheme of successive electron transfer reactions during primary charge separation in bacterial RCs ($P^* \rightarrow P^+B_A^- \rightarrow P^+H_A^- \rightarrow \ldots$) proposed over 30 years ago in the pioneering research of V A Shuvalov and co-workers. The oscillatory character of these dynamics suggests coherence transfer in the form of a wave packet following a similar scheme.

6. Conclusions

The primary act of photosynthesis consists in the conversion of light energy into the energy of separated charges that is utilized in subsequent photosynthetic reactions. The primary act takes place in specialized protein–pigment complexes (reaction centers) in the picosecond range with extremely high ($\sim 100\%$) quantum and rather high ($\sim 50-60\%$) energy efficiencies. Photon absorption in the light-harvesting antenna and RCs themselves excites a specific couple (dimeric bacteriochlorophyll in bacterial RCs) that functions as the final acceptor of the excitation energy and, simultaneously, the primary electron donor P.

The high-rate primary electron transfer in RCs occurs between cofactors of a chlorophyll nature, whose mutual position is supported by the RC protein structure. Each new step of electron transfer is accompanied by a loss of the energy of the initially absorbed quantum in exchange for an extension of time of dissipation of the stored energy; this time exhibits gradual increase at each stage of charge separation. This loss is payment for increasingly more efficient stabilization of an electron on intermediate acceptors with distance from the dimer. As the electron retreats from its primary donor, the energy of interaction between unpaired electrons decreases, and the velocity of the electron's backward motion along vacant orbitals also slows down due to increasing the Boltzmann factor. As a result, the dissipation time of the stored energy increases from ~ 300 ps in the P^* state to ~ 0.1 s in the $P^+Q_A^-$ state.

The maximum rate of direct electron transfer reactions is much higher than that of recombination and relaxation processes; it is a key factor responsible for the high efficiency of the work of RCs and photosynthesis at large. The above factors collectively maintain directional electron transfer in RCs.

The B_A molecule of additional bacteriochlorophyll in bacterial RCs is the primary electron acceptor ensuring the high acceptance rate of electrons from the primary donor P^* and a still higher rate of electron transfer to the next acceptor, bacteriopheophytin H_A. It is achieved due to the smallness or the absence of activation barriers for charge separation reactions and the noticeable overlap of electron orbitals of the participants in these reactions. Achieving the maximally high rates of electron transfer is impossible without the direct involvement of B_A in this process. The nearest environment of the B_A molecule serves the same purpose by accelerating electron transfer. A striking example of such acceleration is

the influence of crystallographic HOH55 water and tyrosine M210 molecules on primary electron transfer. The absence of these molecules in the environment of B_A significantly slows electron transfer. Mechanisms of action of molecules surrounding B_A may consist in the direct influence on energy characteristics of charge separation reactions, participation in dynamic stabilization of separated charges in the $P^+B_A^-$ state, or direct involvement in the spatial electron transfer pathway. A distinctive feature of HOH55 and tyrosine M210 molecules is their polarity, allowing molecular influences to be adjusted in response to the appearance of separated charges, i.e., to maintain the feedback between these mechanisms and the charge separation process.

An important role in electron transfer between reactants is played by vibrations of the nuclear subsystem. Excitation of RCs by femtosecond light pulses induces coherent nuclear motion in the form of a wave packet. This state is an important source of information about the influence of nuclear motion on electron transfer in experiment. Results of femtosecond spectroscopy indicate that the excitation of one of the P electrons is not in itself sufficient to cause charge separation. Only the motion of the nuclear subsystem first in P^* and then in its environment including the B_A molecule results in electron transfer from P^* to B_A with the formation of the primary product $P^+B_A^-$. This motion appears to be aimed at the maximally possible drawing of P^* and B_A together. The momentum acquired as a result of such apposition can be used either to overcome the energy barrier for electron transfer from P^* to B_A or to maintain further motion leading to the spatial separation of the P^+ and B_A^- reaction products. The conjugation (coupling) of motions of nuclear and electron subsystems in this manner is important for the efficient conversion of light energy to the energy of separated charges during photosynthesis. This inference holds true for both the active A-branch and the inactive B-branch of bacterial reaction centers.

Acknowledgments

The authors gratefully acknowledge the invaluable assistance of L G Vasil'eva, V I Novoderezhkin, and A Ya Shkuropatov. The work was supported in part by the Russian Foundation for Basic Research (grant 14-04-00295a).

References

1. Rubin A B, Shinkarev V P *Transport Elektronov v Biologicheskikh Sistemakh* (Electron Transport in Biological Systems) (Moscow: Nauka, 1984)
2. Shuvalov V A *Pervichnoe Preobrazovanie Svetovoi Energii pri Fotosinteze* (The Primary Conversion of Light Energy in Photosynthesis) (Moscow: Nauka, 1990)
3. Deisenhofer J, Norris J R (Eds) *The Photosynthetic Reaction Center* Vols 1, 2 (San Diego, CA: Academic Press, 1993)
4. Parson W W, in *Protein Electron Transfer* (Ed. D S Bendall) (Oxford: BIOS Sci. Publ., 1996) p. 125
5. Hoff A J, Deisenhofer J *Phys. Rep.* **287** 1 (1997)
6. Okamura M Y et al. *Biochim. Biophys. Acta BBA Bioenerg.* **1458** 148 (2000)
7. Shuvalov V A *Preobrazovanie Solnechnoi Energii v Pervichnom Akte Razdeleniya Zaryadov v Reaktsionnykh Tsentrakh Fotosinteza* (Conversion of the Solar Energy in the Primary Act of Charge Separation in Photosynthesis Reaction Centres) (The Timiryazev Readings. Iss. 60) (Moscow: Nauka, 2000)
8. van Brederode M E, Jones M R, in *Enzyme-Catalyzed Electron and Radical Transfer* (Subcellular Biochemistry, Vol. 35, Eds A Holzenburg, N S Scrutton) (New York: Kluwer Acad./Plenum Publ., 2000) p. 621
9. Wraight C A *Front. Biosci.* **9** 309 (2004)
10. Parson W W, Warshel A, in *The Purple Phototrophic Bacteria* (Advances in Photosynthesis and Respiration, Vol. 28, Eds C N Hunter et al.) (Dordrecht: Springer, 2009) p. 355
11. Williams J C, Allen J P, in *The Purple Phototrophic Bacteria* (Advances in Photosynthesis and Respiration, Vol. 28, Eds C N Hunter et al.) (Dordrecht: Springer, 2009) p. 337
12. Yakovlev A G *Pervichnyi Fotosintez* (Primary Photosynthesis) (Saarbrücken: LAMBERT Acad. Publ., 2013)
13. Allakhverdiev S I, Rubin A B, Shuvalov V A (Eds) *Fotosintez: Otkrytye Voprosy i Chto My Znaem Segodnya* (Photosynthesis: Unresolved Problems and What We Know Today) (Moscow–Izhevsk: Inst. Komp'yut. Issled., 2013)
14. Olson J M, Thornber J P, in *Membrane Proteins in Energy Transduction* (Ed. R A Capaldi) (New York: M. Dekker, 1979) p. 279
15. Feher G, Okamura M Y, in *The Photosynthetic Bacteria* (Eds R K Clayton, W R Sistrom) (New York: Plenum Press, 1978) p. 349
16. Deisenhofer J et al. *Nature* **318** 618 (1985)
17. Deisenhofer J, Michel H, Huber R *Trends Biochem.* **10** 243 (1985)
18. Blankenship R E et al. *J. Cell. Biochem.* **22** 251 (1983)
19. Pierson B K, Thornber J P *Proc. Natl. Acad. Sci. USA* **80** 80 (1983)
20. Hale M B, Blankenship R E, Fuller R C *Biochim. Biophys. Acta BBA Bioenerg.* **723** 376 (1983)
21. Michel H et al. *EMBO J.* **5** 1149 (1986)
22. Deisenhofer J et al. *J. Mol. Biol.* **180** 385 (1984)
23. Chang C-H et al. *J. Mol. Biol.* **186** 201 (1985)
24. Chang C-H et al. *FEBS Lett.* **205** 82 (1986)
25. Allen J P et al. *Proc. Natl. Acad. Sci. USA* **84** 5730 (1987)
26. Allen J P et al. *Proc. Natl. Acad. Sci. USA* **84** 6162 (1987)
27. Ermler U et al. *Structure* **2** 925 (1994)
28. Plato M et al., in *The Photosynthetic Bacterial Reaction Center II: Structure, Spectroscopy, and Dynamics* (NATO ASI Ser. A, Vol. 237, Eds J Breton, A Verméglio) (New York: Plenum Press, 1992) p. 109
29. Artz K et al. *Proc. Natl. Acad. Sci. USA* **94** 13582 (1997)
30. Müh F et al. *J. Phys. Chem. B* **106** 3226 (2002)
31. Holten D et al. *Biochim. Biophys. Acta BBA Bioenerg.* **592** 461 (1980)
32. Paschenko V Z et al. *FEBS Lett.* **191** 245 (1985)
33. Woodbury N W et al. *Biochemistry* **24** 7516 (1985)
34. Woodbury N W et al. *Biochemistry* **33** 8101 (1994)
35. Breton J et al. *Proc. Natl. Acad. Sci. USA* **83** 5121 (1986)
36. Martin J-L et al. *Proc. Natl. Acad. Sci. USA* **83** 957 (1986)
37. Wasielewski M R, Tiede D M *FEBS Lett.* **204** 368 (1986)
38. Kirmaier C, Holten D *Israel J. Chem.* **28** 79 (1988)
39. Holzapfel W et al. *Chem. Phys. Lett.* **160** 1 (1989)
40. Holzapfel W et al. *Proc. Natl. Acad. Sci. USA* **87** 5168 (1990)
41. Lauterwasser C et al. *Chem. Phys. Lett.* **183** 471 (1991)
42. Peloquin J M et al. *Biochemistry* **33** 8089 (1994)
43. Holzwarth A R, Muller M G *Biochemistry* **35** 11820 (1996)
44. Huppman P et al. *Biophys. J.* **82** 3186 (2002)
45. Kaufmann K J et al. *Science* **188** 1301 (1975)
46. Rockley M G et al. *Proc. Natl. Acad. Sci. USA* **72** 2251 (1975)
47. Holten D et al. *Biochim. Biophys. Acta BBA Bioenerg.* **501** 112 (1978)
48. Kirmaier C, Holten D, Parson W W *Biochim. Biophys. Acta BBA Bioenerg.* **810** 49 (1985)
49. Kirmaier C, He C, Holten D *Biochemistry* **40** 12132 (2001)
50. Kirmaier C et al. *J. Phys. Chem. B* **108** 11827 (2004)
51. Kellog E C et al. *Photosynth. Res.* **22** 47 (1989)
52. Mar T, Gingras G *Biochim. Biophys. Acta BBA Bioenerg.* **1017** 112 (1990)
53. Robles S J, Breton J, Youvan D C *Science* **248** 1402 (1990)
54. Heller BA, Holten D, Kirmaier C *Science* **269** 940 (1995)
55. de Boer A L et al. *Biochemistry* **41** 3081 (2002)
56. Katilius E et al. *J. Phys. Chem. B* **106** 1471 (2002)
57. Haffa A L M et al. *J. Phys. Chem. B* **108** 4 (2004)
58. Bylina E J et al. *Nature* **336** 182 (1988)
59. Wraight C A, Clayton R K *Biochim. Biophys. Acta BBA Bioenerg.* **333** 246 (1974)
60. Trissl H-W et al. *Biochim. Biophys. Acta BBA Bioenerg.* **1015** 322 (1990)
61. Volk M et al. *J. Phys. Chem. B* **102** 735 (1998)

62. Breton J et al. *Biochemistry* **27** 8276 (1988)
63. Fleming G R, Martin J-L, Breton J *Nature* **333** 190 (1988)
64. Nagarajan V et al. *Proc. Natl. Acad. Sci. USA* **87** 7888 (1990)
65. Nagarajan V et al. *Biochemistry* **32** 12324 (1993)
66. Jia Y et al. *J. Phys. Chem.* **97** 13180 (1993)
67. Haffa A L M et al. *J. Phys. Chem. B* **106** 7376 (2002)
68. Schenck C C et al. *Biophys. J.* **36** 479 (1981)
69. Kirmaier C, Holten D, Parson W W *Biochim. Biophys. Acta BBA Bioenerg.* **810** 33 (1985)
70. Gunner M R, Dutton P L *J. Am. Chem. Soc.* **111** 3400 (1989)
71. Wang H, Lin S, Woodbury N W *J. Phys. Chem. B* **110** 6956 (2006)
72. Lin S et al. *J. Phys. Chem. B* **107** 14103 (2003)
73. Dahlbom M G, Reimers J R *Mol. Phys.* **103** 1057 (2005)
74. Katilius E et al. *J. Phys. Chem. B* **103** 7386 (1999)
75. Katilius E et al. *Photosynth. Res.* **81** 165 (2004)
76. Feick R, Shiozawa J A, Ertlmaier A, in *Anoxygenic Photosynthetic Bacteria* (Advances in Photosynthesis, Vol. 2, Eds R E Blankenship, M T Madigan, C E Bauer) (Dordrecht: Kluwer Acad. Publ., 1995) p. 699
77. Bruce B D, Fuller R C, Blankenship R E *Proc. Natl. Acad. Sci. USA* **79** 6532 (1982)
78. Kirmaier C et al. *FEBS Lett.* **158** 73 (1983)
79. Kirmaier C, Blankenship R E, Holten D *Biochim. Biophys. Acta BBA Bioenerg.* **850** 275 (1986)
80. Vasmel H, Amesz J *Biochim. Biophys. Acta BBA Bioenerg.* **724** 118 (1983)
81. Venturoli G et al. *Eur. J. Biochem.* **202** 625 (1991)
82. Ovchinnikov Yu A et al. *FEBS Lett.* **231** 237 (1988)
83. Ovchinnikov Yu A et al. *FEBS Lett.* **232** 364 (1988)
84. Shiozawa J A et al. *Eur. J. Biochem.* **180** 75 (1989)
85. Parot P et al. *Biochim. Biophys. Acta BBA Bioenerg.* **809** 137 (1985)
86. Shuvalov V A et al. *Biochim. Biophys. Acta BBA Bioenerg.* **849** 337 (1986)
87. Vasmel H, Amesz J, Hoff A J *Biochim. Biophys. Acta BBA Bioenerg.* **852** 159 (1986)
88. Scherer P O J, Fischer S F *Biochim. Biophys. Acta BBA Bioenerg.* **891** 157 (1987)
89. Becker M et al. *Biochim. Biophys. Acta BBA Bioenerg.* **1057** 299 (1991)
90. Feick R et al., in *Reaction Centers of Photosynthetic Bacteria. Feldafing-II-Meeting* (Springer Series in Biophysics, Vol. 6, Ed. M E Michel-Beyerle) (Berlin: Springer-Verlag, 1990) p. 181
91. Volk M et al. *Biochim. Biophys. Acta BBA Bioenerg.* **1058** 217 (1991)
92. Wachtveitl J et al. *Spectrochim. Acta A* **54** 1231 (1998)
93. Parson W W, Chu Z-T, Warshel A *Biochim. Biophys. Acta BBA Bioenerg.* **1017** 251 (1990)
94. Gunner M, Nicholls A, Honig B *J. Phys. Chem.* **100** 4277 (1996)
95. Watanabe T, Kobayashi M, in *Chlorophylls* (Ed. H Scheer) (Boca Raton, Fla.: CRC Press, 1991) p. 287
96. Fajer J et al. *Proc. Natl. Acad. Sci. USA* **72** 4956 (1975)
97. Schweitzer G et al. *Chem. Phys. Lett.* **190** 149 (1992)
98. Aumeier W et al., in *Current Research in Photosynthesis. Proc. of the VIIIth Intern. Congress on Photosynthesis, Stockholm, Sweden, August 6–11, 1989* (Ed. M Baltscheffsky) Vol. 1 (Dordrecht: Kluwer Acad. Publ., 1990) p. 133
99. van Brederode M E et al. *Biochemistry* **36** 6855 (1997)
100. van Brederode M E et al. *Proc. Natl. Acad. Sci. USA* **96** 2054 (1999)
101. van Brederode M E et al. *Biochemistry* **38** 7545 (1999)
102. Lin S et al. *J. Phys. Chem. B* **103** 4757 (1999)
103. Lin S et al. *Biochemistry* **40** 13767 (2001)
104. Zhou H, Boxer S G *J. Phys. Chem. B* **102** 9139 (1998)
105. Zhou H, Boxer S G *J. Phys. Chem. B* **102** 9148 (1998)
106. King B A et al. *J. Phys. Chem. B* **105** 1856 (2001)
107. Kennis J T M et al. *Biochemistry* **36** 16231 (1997)
108. Shuvalov V A, Parson W W *Proc. Natl. Acad. Sci. USA* **78** 957 (1980)
109. Vos M H et al. *Proc. Natl. Acad. Sci. USA* **88** 8885 (1991)
110. Vos M H et al. *Proc. Natl. Acad. Sci. USA* **89** 613 (1992)
111. Du M et al. *Proc. Natl. Acad. Sci. USA* **89** 8517 (1992)
112. Hamm P et al. *Biochim. Biophys. Acta BBA Bioenerg.* **1142** 99 (1993)
113. Stanley R J, Boxer S G *J. Phys. Chem.* **99** 859 (1995)
114. Beekman L M P et al. *J. Phys. Chem.* **100** 7256 (1996)
115. Ogrodnik A et al. *Chem. Phys.* **244** 461 (1999)
116. Wang H W et al. *Science* **316** 747 (2007)
117. Kirmaier C, Holten D *Proc. Natl. Acad. Sci. USA* **87** 3552 (1990)
118. Wang Z et al. *Chem. Phys.* **176** 421 (1993)
119. Gehlen J N, Marchi M, Chandler D *Science* **263** 499 (1994)
120. Hartwich G et al. *J. Phys. Chem. B* **102** 3815 (1998)
121. Peloquin J M et al. *J. Phys. Chem.* **99** 1349 (1995)
122. Peloquin J M et al. *J. Phys. Chem.* **100** 14228 (1996)
123. Small G J, Hayes J M, Silbey R J *J. Phys. Chem.* **96** 7499 (1992)
124. Lyle P A, Kolaczkowski S V, Small G J *J. Phys. Chem.* **97** 6924 (1993)
125. Small G J *Chem. Phys.* **197** 239 (1995)
126. Hamm P, Zinth W *J. Phys. Chem.* **99** 13537 (1995)
127. Johnson S G et al. *J. Phys. Chem.* **94** 5849 (1990)
128. Middendorf T R et al. *J. Phys. Chem.* **95** 10142 (1991)
129. Reddy N R S, Lyle P A, Small G J *Photosynth. Res.* **31** 167 (1992)
130. Vos M H et al. *Nature* **363** 320 (1993)
131. Vos M H et al. *Proc. Natl. Acad. Sci. USA* **91** 12701 (1994)
132. Vos M H et al. *Biochemistry* **33** 6750 (1994)
133. Vos M H et al. *Biochemistry* **35** 2687 (1996)
134. Vos M H, Jones M R, Martin J-L *Chem. Phys.* **233** 179 (1998)
135. Vos M H et al. *Biochemistry* **39** 8353 (2000)
136. Martin J-L, Vos M H *Annu. Rev. Biophys. Biomol. Struct.* **21** 199 (1992)
137. Vos M, Martin J-L *Biochim. Biophys. Acta BBA Bioenerg.* **1411** 1 (1999)
138. Spörlein S, Zinth W, Wachtveitl J *J. Phys. Chem. B* **102** 7492 (1998)
139. Rischel C et al. *Proc. Natl. Acad. Sci. USA* **95** 12306 (1998)
140. Parson W W, Warshel A *Chem. Phys.* **296** 201 (2004)
141. Parson W W, Warshel A *J. Phys. Chem. B* **108** 10474 (2004)
142. Czarnecki K et al. *J. Am. Chem. Soc.* **119** 415 (1997)
143. Kitzing E, Kühn H *J. Phys. Chem.* **94** 1699 (1990)
144. Lin S, Taguchi A K W, Woodbury N W *J. Phys. Chem.* **100** 17067 (1996)
145. Taguchi A K W et al. *Biochemistry* **35** 3175 (1996)
146. Wakeham M C, Jones M R *Biochem. Soc. Trans.* **133** 851 (2005)
147. Kirmaier C et al. *J. Phys. Chem. B* **106** 495 (2002)
148. Kirmaier C et al. *J. Phys. Chem. B* **106** 1799 (2002)
149. Kirmaier C et al. *Biochemistry* **42** 2016 (2003)
150. Kee H L et al. *Biochemistry* **45** 7314 (2006)
151. Paddock M L et al. *Biochemistry* **45** 14032 (2006)
152. Laible P D et al. *Biochemistry* **42** 1718 (2003)
153. Breton J et al. *Biochim. Biophys. Acta BBA Bioenerg.* **1656** 127 (2004)
154. Paddock M L et al. *Biochemistry* **44** 6920 (2005)
155. Wakeham M C et al. *FEBS Lett.* **540** 234 (2003)
156. Wakeham M C et al. *Biochemistry* **43** 4755 (2004)
157. Frolov D et al. *Biochim. Biophys. Acta BBA Bioenerg.* **1707** 189 (2005)
158. Allen J P et al. *Photosynth. Res.* **55** 227 (1998)
159. Parson W W, Warshel A, in *Biophysical Techniques in Photosynthesis* Vol. 2 (Advances in Photosynthesis and Respiration, Vol. 26, Eds T J Aartsma, J Matysik) (Dordrecht: Springer, 2008) p. 401
160. Warshel A, Parson W W *Quart. Rev. Biophys.* **34** 563 (2001)
161. Alden R G et al. *J. Phys. Chem.* **100** 16761 (1996)
162. Finkele U et al. *Biochemistry* **29** 8517 (1990)
163. Chan C K et al. *Chem. Phys. Lett.* **176** 366 (1991)
164. Shochat S et al. *Photosynth. Res.* **40** 55 (1994)
165. Heller B A, Holten D, Kirmaier C *Biochemistry* **34** 5294 (1995)
166. Heller B A, Holten D, Kirmaier C *Biochemistry* **35** 15418 (1996)
167. Kirmaier C et al. *J. Phys. Chem.* **99** 8903 (1995)
168. Kirmaier C et al. *J. Phys. Chem.* **99** 8910 (1995)
169. Kirmaier C, Weems D, Holten D *Biochemistry* **38** 11516 (1999)
170. Lin S et al. *Biochemistry* **35** 3187 (1996)
171. Czarnecki K et al. *J. Phys. Chem. A* **103** 2235 (1999)
172. Chuang J I et al. *Biochemistry* **45** 3845 (2006)
173. Ivashin N et al. *J. Phys. Chem. B* **102** 5017 (1998)
174. Kolbasov D, Scherz A, in *Photosynthesis: Mechanisms and Effects. Proc. of the XIth Intern. Congress on Photosynthesis, Budapest, Hungary, August 17–22, 1998* Vol. 2 (Ed. G Garab) (Dordrecht: Kluwer Acad. Publ., 1998) p. 719
175. Kolbasov D, Scherz A *J. Phys. Chem. B* **104** 1802 (2000)
176. Zhang L Y, Friesner R A *Proc. Natl. Acad. Sci. USA* **95** 13603 (1998)

177. Parson W W, Creighton S, Warshel A, in *Primary Processes in Photobiology. Proc. of the 12th Taniguchi Symp., Fujiyoshida, Yamanashi Prefecture, Japan, December 7 – 12, 1986* (Ed. T Kobayashi) (Berlin: Springer-Verlag, 1987) p. 43
178. Warshel A, Creighton S, Parson W W *J. Phys. Chem.* **92** 2698 (1988)
179. Moser C C et al. *Nature* **355** 796 (1992)
180. Gray H B, Winkler J R *Annu. Rev. Biochem.* **65** 537 (1996)
181. Newton M D *Theor. Chem. Acc.* **110** 307 (2003)
182. Skourtis S S et al. *Proc. Natl. Acad. Sci. USA* **102** 3552 (2005)
183. Steffen M A, Lao K Q, Boxer S G *Science* **264** 810 (1994)
184. Lin J, Beratan D N *J. Phys. Chem. B* **109** 7529 (2005)
185. Gray H B, Winkler J R *Proc. Natl. Acad. Sci. USA* **102** 3534 (2005)
186. Noy D, Moser C C, Dutton P L *Biochim. Biophys. Acta BBA Bioenerg.* **1757** 90 (2006)
187. Katilius E et al. *J. Phys. Chem. B* **106** 12344 (2002)
188. Kirmaier C et al. *J. Phys. Chem. B* **109** 24160 (2005)
189. Ishikita H et al. *FEBS Lett.* **579** 712 (2005)
190. Ishikita H et al. *Biochemistry* **45** 2063 (2006)
191. Middendorf T R et al. *Biochim. Biophys. Acta BBA Bioenerg.* **1143** 223 (1993)
192. Yanagi K et al. *J. Phys. Chem. B* **109** 992 (2005)
193. Haffa A L M et al. *J. Phys. Chem. B* **107** 12503 (2003)
194. Yakovlev A G et al. *Biochim. Biophys. Acta BBA Bioenerg.* **1757** 369 (2006)
195. Yakovlev A G et al. *J. Bioinform. Comput. Biol.* **6** 643 (2008)
196. McDowell L M et al. *Biochemistry* **30** 8315 (1991)
197. Allen J P et al. *Biochemistry* **35** 6612 (1996)
198. Kirmaier C et al. *Science* **251** 922 (1991)
199. Watson A J et al. *Biochim. Biophys. Acta BBA Bioenerg.* **1710** 34 (2005)
200. Williams J C et al. *Appl. Magn. Reson.* **31** 45 (2007)
201. Jackson J A et al. *J. Phys. Chem. B* **101** 5747 (1997)
202. Moore L J, Boxer S G *Photosynth. Res.* **55** 173 (1998)
203. Robles S J, Breton J, Youvan D C, in *Reaction Centers of Photosynthetic Bacteria. Feldafing-II-Meeting* (Springer Series in Biophysics, Vol. 6, Ed. M-E Michel-Beyerle) (Berlin: Springer-Verlag, 1990) p. 283
204. Khatypov R A et al. *Biochemistry Moscow* **70** 1527 (2005)
205. Spiedel D, Jones M R, Robert B *FEBS Lett.* **527** 171 (2002)
206. Stocker J W et al. *Biochemistry* **31** 10356 (1992)
207. Williams J C et al. *Biochemistry* **31** 11029 (1992)
208. Murchison H A et al. *Biochemistry* **32** 3498 (1993)
209. Allen J P, Williams J C *J. Bioenerg. Biomembr.* **27** 275 (1995)
210. Allen J P, Williams J C, in *Chlorophylls and Bacteriochlorophylls: Biochemistry, Biophysics, Functions and Applications* (Advances in Photosynthesis and Respiration, Vol. 25, Eds B Grimm et al.) (Dordrecht: Springer, 2006) p. 283
211. Lin X et al. *Proc. Natl. Acad. Sci. USA* **91** 10265 (1994)
212. Chen L et al. *J. Phys. Chem. B* **108** 10457 (2004)
213. Müh F et al. *Biochemistry* **37** 13066 (1998)
214. Williams J C et al. *Biochemistry* **40** 15403 (2001)
215. Johnson E T, Parson W W *Biochemistry* **41** 6483 (2002)
216. Johnson E T et al. *J. Phys. Chem. B* **106** 11859 (2002)
217. Treynor T P, Yoshina-Ishii C, Boxer S G *J. Phys. Chem. B* **108** 13523 (2004)
218. Alden R G et al., in *Reaction Centers of Photosynthetic Bacteria: Structure and Dynamics* (Ed. M-E Michel-Beyerle) (Berlin: Springer, 1996) p. 105
219. Reimers J R, Hush N S *J. Am. Chem. Soc.* **126** 4132 (2004)
220. Kanchanawong P et al. *J. Phys. Chem. B* **110** 18688 (2006)
221. Goldsmith J O, Boxer S G *Biochim. Biophys. Acta BBA Bioenerg.* **1276** 171 (1996)
222. Bylina E J et al. *Biochemistry* **29** 6203 (1990)
223. Arlt T et al. *J. Phys. Chem.* **100** 12060 (1996)
224. Arlt T et al. *Biochemistry* **35** 9235 (1996)
225. Katilius E et al. *J. Phys. Chem. B* **107** 12029 (2003)
226. Bylina E J, Youvan D C *Proc. Natl. Acad. Sci. USA* **85** 7226 (1988)
227. Kálmán L et al. *Nature* **402** 696 (1999)
228. Kálmán L et al. *Biochemistry* **42** 13280 (2003)
229. Narváez A J et al. *Biochemistry* **41** 15253 (2002)
230. Narváez A J et al. *Biochemistry* **43** 14379 (2004)
231. Thielges M et al. *Biochemistry* **44** 7389 (2005)
232. Kálmán L et al. *Biochemistry* **44** 13266 (2005)
233. Johnson E T et al. *Biochemistry* **42** 13673 (2003)
234. de Boer A L et al. *Photosynth. Res.* **71** 221 (2002)
235. Woodbury N W et al. *Chem. Phys.* **197** 405 (1995)
236. McAuley K E et al. *FEBS Lett.* **467** 285 (2000)
237. Yakovlev A G et al. *J. Phys. Chem. A* **107** 8330 (2003)
238. Yakovlev A G et al. *Biochemistry Moscow* **74** 1203 (2009); *Biokhimiya* **74** 1479 (2009)
239. Yakovlev A G et al. *Biochemistry Moscow* **75** 832 (2010); *Biokhimiya* **75** 944 (2010)
240. Pawlowicz N P et al. *Phys. Chem. Chem. Phys.* **12** 2693 (2010)
241. Plato M et al., in *The Photosynthetic Bacterial Reaction Center: Structure and Dynamics* (NATO ASI Series A, Vol. 149, Eds J Breton, A Vermeglio) (New York: Plenum Press, 1988) p. 379
242. Yakovlev A G, Shkuropatov A Ya, Shuvalov V A *Biochemistry* **41** 14019 (2002)
243. Yakovlev A G, Shkuropatov A Ya, Shuvalov V A *Biochemistry* **41** 2667 (2002)
244. Fok M V, Borisov A Yu *Mol. Biol.* **15** 575 (1981)
245. Yakovlev A G et al. *Chem. Phys.* **319** 297 (2005)
246. Potter J A et al. *J. Biol. Chem.* **280** 27155 (2005)
247. Deisenhofer J et al. *J. Mol. Biol.* **246** 429 (1995)
248. Stowell M H B et al. *Science* **276** 812 (1997)
249. Fyfe P K et al. *Biochemistry* **39** 5953 (2000)
250. Herzberg G *Infrared and Raman Spectra of Polyatomic Molecules* (New York: Van Nostrand, 1945); Translated into Russian: *Kolebatel'nye i Vrashchatel'nye Spektry Mnogoatomnykh Molekul* (Moscow: IL, 1949)
251. de Rege P J F, Williams S A, Therien M J *Science* **269** 1409 (1995)
252. Bixon M, Jortner J, Michel-Beyerle M E *Biochim. Biophys. Acta BBA Bioenerg.* **1056** 301 (1991)
253. Creighton S et al. *Biochemistry* **27** 774 (1988)
254. Alden R G et al. *J. Am. Chem. Soc.* **117** 12284 (1995)
255. Warshel A et al. *Biochim. Biophys. Acta BBA Bioenerg.* **1764** 1647 (2006)
256. Scherer P O J, Fischer S F *J. Phys. Chem.* **93** 1633 (1989)
257. Scherer P O J, Fischer S F *Spectrochim. Acta A* **54** 1191 (1998)
258. Thompson M A, Zerner M C, Fajer J *J. Am. Chem. Soc.* **113** 8210 (1991)
259. Marchi M et al. *J. Am. Chem. Soc.* **115** 4178 (1993)
260. Blomberg M R A, Siegbahn P H M, Babcock G T *J. Am. Chem. Soc.* **120** 8812 (1998)
261. Hasegawa J, Nakatsuji H *J. Phys. Chem. B* **102** 10420 (1998)
262. Hughes J M et al. *J. Am. Chem. Soc.* **123** 8550 (2001)
263. Gilson M K et al. *J. Mol. Biol.* **184** 503 (1985)
264. Warshel A, Russell S T *Quart. Rev. Biophys.* **17** 283 (1984)
265. Hunenberger P H, Mark A E, van Gunsteren W F *J. Mol. Biol.* **252** 492 (1995)
266. Figueirido F, Del Buono G S, Levy R M *J. Phys. Chem. B* **101** 5622 (1997)
267. Sham Y Y, Warshel A *J. Chem. Phys.* **109** 7940 (1998)
268. Procacci et al. *J. Comp. Chem.* **18** 1848 (1997)
269. Ceccarelli M, Marchi M *J. Phys. Chem. B* **107** 5630 (2003)
270. Parson W W, Chu Z T, Warshel A *Biophys. J.* **74** 182 (1998)
271. Parson W W, Chu Z T, Warshel A *Photosynth. Res.* **55** 147 (1998)
272. Schmidt S et al. *Chem. Phys. Lett.* **223** 116 (1994)
273. Schmidt S et al. *Spectrochim. Acta A* **51** 1565 (1995)
274. Egger R, Mak C H *J. Phys. Chem.* **98** 9903 (1994)
275. Bixon M, Jortner J, Michel-Beyerle M E *Chem. Phys.* **197** 389 (1995)
276. Bixon M, Jortner J, Michel-Beyerle M E, in *The Reaction Center of Photosynthetic Bacteria: Structure and Dynamics* (Ed. M-E Michel-Beyerle) (Berlin: Springer, 1996) p. 287
277. Sim E, Makri N *J. Phys. Chem. B* **101** 5446 (1997)
278. Zusman L D, Beratan D N *Spectrochim. Acta A* **54** 1211 (1998)
279. Spörlein S et al. *Chem. Phys. Lett.* **322** 454 (2000)
280. Roberts J A, Holten D, Kirmaier C *J. Phys. Chem. B* **105** 5575 (2001)
281. Ivashin N, Larsson S *J. Phys. Chem. B* **106** 3996 (2002)
282. Shuvalov V A, Yakovlev A G *Biochemistry Moscow Suppl. A* **12** 563 (1998); *Biol. Membr.* **15** 459 (1998)
283. Shuvalov V A, Klimov V V *Biochim. Biophys. Acta BBA Bioenerg.* **440** 587 (1976)
284. Godik V I, Borisov A Y *Biochim. Biophys. Acta BBA Bioenerg.* **548** 296 (1979)
285. Rademaker J, Hoff A J *Biophys. J.* **34** 325 (1981)

286. Godik V I, Kotova E A, Borisov A Y *Photobiochem. Photobiophys.* **4** 219 (1982)
287. Schenck C C, Blankenship R E, Parson W W *Biochim. Biophys. Acta BBA Bioenerg.* **680** 44 (1982)
288. Woodbury N W T, Parson W W *Biochim. Biophys. Acta BBA Bioenerg.* **767** 345 (1984)
289. Hörber J K H et al. *FEBS Lett.* **198** 273 (1986)
290. Woodbury N W et al. *Biochim. Biophys. Acta BBA Bioenerg.* **851** 6 (1986)
291. Goldstein R A, Boxer S G *Biochim. Biophys. Acta BBA Bioenerg.* **977** 70 (1988)
292. Ogrodnik A *Biochim. Biophys. Acta BBA Bioenerg.* **1020** 65 (1990)
293. Ogrodnik A et al. *J. Phys. Chem.* **98** 3432 (1994)
294. Parson W W, Clayton R K, Cogdell R J *Biochim. Biophys. Acta BBA Bioenerg.* **387** 265 (1975)
295. Takiff L, Boxer S G *Biochim. Biophys. Acta BBA Bioenerg.* **932** 325 (1988)
296. Blankenship R E, Schaafsma T J, Parson W W *Biochim. Biophys. Acta BBA Bioenerg.* **461** 297 (1977)
297. Haberkorn R, Michel-Beyerle M E *Biophys. J.* **26** 489 (1979)
298. Hoff A J *Quart. Rev. Biophys.* **14** 599 (1981)
299. Boxer S G, Chidsey E D, Roelofs M G *Annu. Rev. Phys. Chem.* **34** 389 (1983)
300. Chidsey C E D et al. *Proc. Natl. Acad. Sci. USA* **82** 6850 (1985)
301. Ogrodnik A et al. *Biochim. Biophys. Acta BBA Bioenerg.* **936** 361 (1988)
302. Boxer S G et al. *J. Phys. Chem.* **93** 8280 (1989)
303. Shuvalov V A et al. *FEBS Lett.* **91** 135 (1978)
304. Shuvalov V A, Duysens L N M *Proc. Natl. Acad. Sci. USA* **83** 1690 (1986)
305. Chekalin S V et al. *FEBS Lett.* **216** 245 (1987)
306. Matveets Yu A et al. *Dokl. Akad. Nauk SSSR* **294** 1480 (1987)
307. Arlt T et al. *Proc. Natl. Acad. Sci. USA* **9**0 11757 (1993)
308. Bixon M et al., in *The Photosynthetic Bacterial Reaction Center: Structure and Dynamics* (NATO ASI Series A, Vol. 149, Eds J Breton, A Vermeglio) (New York: Plenum Press, 1988) p. 399
309. van Stokkum I H M et al. *Biochemistry* **36** 11360 (1997)
310. Shkuropatov A Y, Shuvalov V A *FEBS Lett.* **322** 168 (1993)
311. Yakovlev A G, Shkuropatov A Ya, Shuvalov V A *FEBS Lett.* **466** 209 (2000)
312. Redfield A G, in *Advances in Magnetic Resonance* Vol. 1 (Ed. J S Waugh) Vol. 1 (New York: Academic Press, 1965) p. 1
313. Novoderezhkin V I et al. *J. Phys. Chem. B* **108** 7445 (2004)
314. Eisenmayer T J et al. *J. Phys. Chem. Lett.* **3** 694 (2012)
315. Eisenmayer T J et al. *J. Phys. Chem. B* **117** 11162 (2013)
316. Milanovsky G E et al. *J. Phys. Chem. B* **119** 13656 (2015)
317. Cherepy N J et al. *J. Phys. Chem.* **98** 6023 (1994)
318. Cherepy N J et al. *Biochemistry* **36** 8559 (1997)